POLITECNICO DI TORINO

Mechanical and Aerospace Engineering Department

Master of Science Program in Automotive Engineering

Experimental Validation and Robustness Analysis of a Hybrid EKF–Neural Network Framework for SOC Estimation in LFP Lithium-Ion Batteries

Supervisors

Davide Papurello, Associate Professor

Francesco Demetrio Minuto, Assistant Professor

Co-supervisors

Lorenzo Giannuzzo, PhD Candidate

Marcel Stolte, PhD Candidate

Candidate

Javodulla Khasankhonov

A.A 2025/2026

Abstract

Accurate state-of-charge (SOC) estimation is a critical requirement for the safe and efficient operation of lithium iron phosphate (LFP) battery systems. However, the characteristic flat open-circuit voltage (OCV) profile of LFP chemistry significantly reduces voltage sensitivity to SOC variations, limiting the effectiveness of purely voltage-based estimation methods, particularly under dynamic operating conditions. While data-driven approaches can achieve high estimation accuracy, they often lack physical interpretability and robustness. Conversely, model-based observers maintain consistency with battery physics but may suffer from performance degradation due to modeling inaccuracies and parameter uncertainties.

This thesis develops, implements, and experimentally validates a hybrid SOC estimation framework that integrates an equivalent circuit model (R0+1RC) with an Extended Kalman Filter (EKF) and a neural-network-based correction layer. The proposed workflow follows a structured and modular pipeline including dataset preprocessing and reference SOC reconstruction, open-circuit voltage characterization, equivalent circuit model parameterization, EKF-based state estimation, and supervised learning of residual SOC errors using a recurrent neural network based on a gated recurrent unit (GRU) architecture.

The framework is validated using experimental datasets obtained from an LFP battery cell under controlled charge–discharge cycling conditions. Estimation performance is evaluated through a cycle-based training, validation, and testing protocol, with separate analysis of charge and discharge operating regimes. The results demonstrate that the hybrid estimator consistently reduces SOC root mean square error (RMSE) compared with a standalone EKF estimator, while preserving physical interpretability and numerical stability.

Special attention is devoted to robustness analysis, including the influence of OCV slope regions, operating regimes, and dataset composition on estimation performance. The proposed framework provides a reproducible and experimentally validated methodology for hybrid SOC estimation in LFP batteries and establishes a foundation for future extensions toward highly dynamic operating profiles and advanced battery management applications.

List of Figures

List of Tables

Table of Contents

1. Introduction

The rapid electrification of transportation and the increasing integration of renewable energy sources have significantly accelerated the development and deployment of lithium-ion battery technologies [1], [2]. In electric vehicles (EVs), the battery system represents the primary energy storage component and directly influences vehicle range, safety, performance, and durability. To ensure safe and reliable operation, modern battery systems rely on a Battery Management System (BMS) that continuously monitors and estimates internal battery states that cannot be directly measured. Among these variables, the state of charge (SOC) is one of the most critical parameters for energy management and safe operation.

Accurate SOC estimation is essential for preventing overcharge and overdischarge, optimizing energy utilization, and ensuring reliable system operation. However, SOC cannot be directly measured and must instead be estimated using mathematical models or data-driven inference. Classical model-based approaches, particularly those based on equivalent circuit models combined with Kalman filtering techniques, have been widely adopted due to their solid theoretical foundation and suitability for real-time implementation in embedded battery management systems [3], [4], [8]. Early work by Plett established the theoretical basis for Kalman-filter-based SOC estimation in lithium-ion batteries and remains one of the most widely referenced approaches in the field [3], [14]. Subsequent studies further evaluated equivalent circuit models and observer structures for practical BMS implementation [8], [10], [11].

Despite their advantages, model-based estimation methods strongly depend on accurate model parameterization and may experience performance degradation under nonlinear operating conditions, parameter uncertainties, or aging-related changes in battery characteristics. Battery degradation mechanisms, including capacity fade and resistance growth, further complicate the estimation problem and require adaptive modeling strategies [12], [25].

In parallel, data-driven approaches based on machine learning have demonstrated strong capabilities in modeling complex nonlinear relationships between measurable battery signals and internal states. Neural networks, particularly recurrent architectures, have shown promising results in battery state estimation due to their ability to capture temporal dependencies in time-series data [18], [19], [20]. Hybrid approaches combining neural networks with filtering techniques have also been investigated to improve estimation accuracy [21], [27], [28], [29], [30]. Consequently, hybrid approaches that integrate model-based observers with data-driven correction mechanisms have recently emerged as an effective strategy for improving SOC estimation performance [5], [6], [7].

SOC estimation becomes particularly challenging in lithium iron phosphate (LFP) batteries. Although LFP chemistry offers several advantages such as high thermal stability, long cycle life, and relatively low cost, it introduces specific difficulties for voltage-based estimation methods. In particular, LFP batteries exhibit a characteristic flat region in the open-circuit voltage (OCV) curve over a wide SOC range, meaning that large SOC variations correspond to only small voltage changes [6], [23]. This reduced voltage sensitivity significantly limits the observability of SOC in model-based observers. In addition, voltage hysteresis and relaxation dynamics further complicate

the relationship between terminal voltage and SOC, increasing the difficulty of accurate state reconstruction [24].

These challenges motivate the development of advanced estimation frameworks capable of improving SOC accuracy under the specific characteristics of LFP batteries. Hybrid estimation approaches that combine the physical consistency of model-based observers with the nonlinear approximation capability of neural networks represent a promising direction for addressing these limitations.

The objective of this thesis is therefore to develop and experimentally validate a hybrid SOC estimation framework for lithium iron phosphate batteries. The proposed approach integrates a model-based Extended Kalman Filter with a recurrent neural network based on a gated recurrent unit (GRU) architecture. In this framework, the EKF provides a physically interpretable baseline estimate, while the neural network learns structured residual errors and refines the SOC estimation.

The performance of the proposed hybrid framework is evaluated using an experimental dataset obtained from an 18650 LFP battery cell. The estimation accuracy of the hybrid method is compared with classical approaches, including Coulomb counting and standalone EKF estimation.

The remainder of this thesis is organized as follows. Chapter 2 reviews the state of the art and the theoretical background related to LFP battery characteristics, battery internal states, SOC estimation methods, and hybrid estimation approaches. Chapter 3 presents the SOC estimation framework, including dataset preprocessing, reference SOC construction, baseline estimators, and the proposed hybrid EKF–GRU architecture. Chapter 4 describes the experimental validation methodology and reports the estimation results. Chapter 5 discusses the obtained results and their implications for SOC estimation in LFP batteries. Finally, Chapter 6 concludes the thesis and Chapter 7 outlines potential directions for future work.

2. State of the Art and Theoretical Background

This chapter reviews the current state of the art in battery state estimation and introduces the theoretical foundations required for the development of the proposed hybrid SOC estimation framework. The chapter begins with a brief overview of lithium iron phosphate (LFP) battery characteristics and the challenges they introduce for state estimation. Subsequently, the main battery internal states relevant to battery management systems are introduced. Finally, the chapter reviews the principal categories of SOC estimation methods, including model-based observers and neural-network-based approaches, and discusses the motivation for hybrid estimation strategies.

2.1. Lithium Iron Phosphate Battery Characteristics

Lithium iron phosphate ($LiFePO_4$, LFP) batteries have become widely adopted in electric mobility and stationary energy storage systems due to their intrinsic safety, long cycle life, thermal stability, and relatively low cost [6], [23]. Compared with other lithium-ion chemistries such as nickel-manganese-cobalt (NMC) or nickel-cobalt-aluminum (NCA), LFP batteries demonstrate excellent thermal stability and resistance to thermal runaway, making them particularly attractive for large-scale energy storage applications.

Despite these advantages, LFP chemistry presents several challenges for battery state estimation algorithms. These challenges arise primarily from the electrochemical characteristics of the cathode material and the resulting voltage behavior.

2.1.1. Open-Circuit Voltage Characteristics

One of the most distinctive characteristics of LFP batteries is the presence of a pronounced flat region in the open-circuit voltage (OCV) versus SOC relationship. In contrast to other lithium-ion chemistries that exhibit a steep and monotonic OCV–SOC curve, LFP cells maintain an almost constant voltage over a wide SOC range, typically between approximately 30% and 80% SOC [6], [24].

In this plateau region, the derivative of the OCV curve with respect to SOC becomes very small:

$$\frac{dOCV}{dSOC} \approx 0$$

As a consequence, even small voltage measurement noise can produce large uncertainties in SOC estimation when relying on voltage-based inversion methods.

This plateau behavior originates from the two-phase reaction mechanism of the $LiFePO_4$ cathode material and has been extensively discussed in electrochemical modeling studies of lithium-ion batteries [24], [25].

This property significantly reduces the observability of SOC in estimation algorithms that rely on voltage measurements, such as Kalman-filter-based observers.

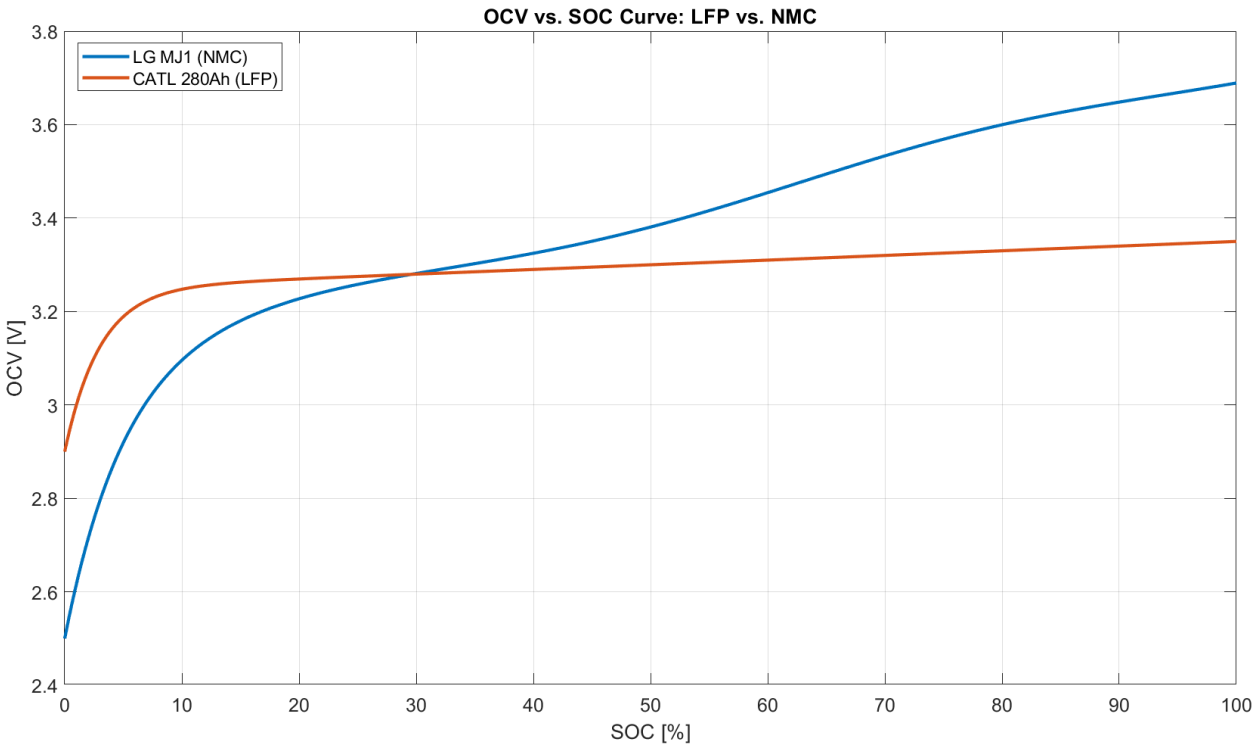

Figure 1: OCV–SOC characteristics of LFP vs. NMC lithium-ion batteries.

2.1.2. Hysteresis Behavior

Another important characteristic of LFP batteries is voltage hysteresis. The terminal voltage corresponding to a given SOC differs depending on whether the battery is undergoing charging or discharging. This phenomenon originates from the two-phase electrochemical transition occurring in the $LiFePO_4$ cathode material [24].

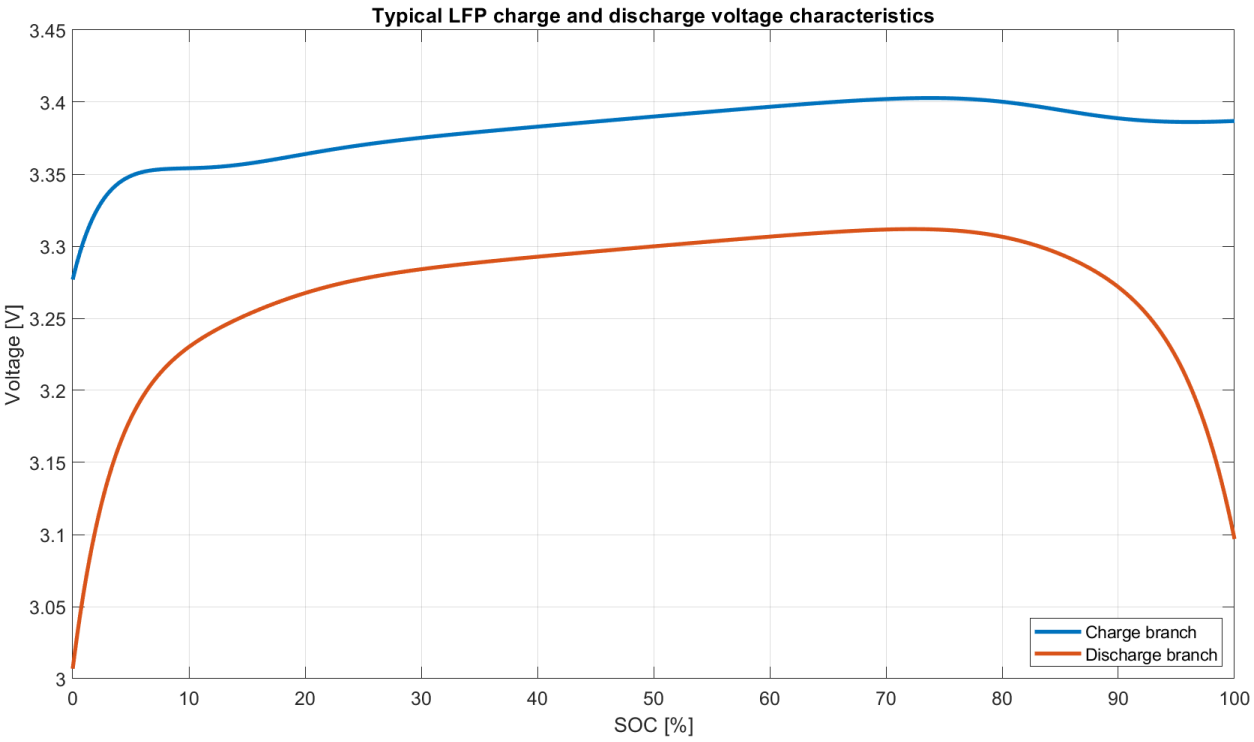

Figure 2: Typical LFP voltage plateau during charge and discharge.

As shown in the figure, the voltage curves corresponding to the two operating modes are separated, reflecting the presence of hysteresis in the electrochemical process.

As a consequence, the terminal voltage cannot be represented as a single-valued function of SOC. Instead, it depends on both the direction of the current and the previous operating history of the cell. If hysteresis effects are not explicitly considered in the modeling process, voltage-based SOC estimators may exhibit systematic bias, particularly during transitions between charging and discharging conditions.

2.1.3. Relaxation Dynamics and Aging Effects

After current interruption, the terminal voltage of lithium-ion batteries gradually relaxes toward its equilibrium open-circuit value. For LFP cells, this relaxation process can be relatively slow, with deviations from equilibrium persisting even after long rest periods [6].

In addition, battery aging introduces changes in internal resistance and capacity fade, which influence both the process and measurement equations of state estimation models [12], [25].

The combination of flat OCV behavior, hysteresis effects, and aging-induced parameter drift makes SOC estimation in LFP batteries particularly challenging.

2.2. Battery Internal States in Battery Management Systems

Battery management systems rely on the estimation of several internal states that cannot be directly measured. These states provide critical information for energy management, safety monitoring, and lifetime prediction.

Among the various battery internal variables, two states play a central role in battery management systems: the state of charge (SOC) and the state of health (SOH).

2.2.1. State of Charge (SOC)

The state of charge represents the ratio between the remaining available capacity and the nominal capacity of the battery. It can be expressed as

$$SOC = \frac{Q_{remaining}}{Q_{nominal}}$$

where $Q_{remaining}$ denotes the available charge in the battery and $Q_{nominal}$ is the nominal capacity.

SOC is one of the most important variables monitored by the battery management system, as it determines the remaining driving range in electric vehicles and prevents unsafe operating conditions such as overcharge or deep discharge.

However, SOC cannot be measured directly. Instead, it must be estimated from measurable electrical quantities such as current and voltage.

2.2.2. State of Health (SOH)

The state of health quantifies the degradation level of the battery compared with its original condition. It is typically defined as

$$SOH = \frac{Q_{current}}{Q_{nominal}}$$

where $Q_{current}$ represents the current maximum discharge capacity.

Battery aging gradually reduces available capacity and increases internal resistance. Accurate SOH estimation is therefore essential for predicting remaining useful life and maintaining safe system operation.

Although SOH estimation is an important research topic, this thesis primarily focuses on SOC estimation while assuming known nominal capacity.

2.3. State-of-the-Art SOC Estimation Methods

Over the past two decades, numerous methods for estimating the state of charge (SOC) of lithium-ion batteries have been proposed. These approaches can generally be grouped into several main categories, including classical integration-based techniques, model-based observers, data-driven methods, and hybrid estimation frameworks.

Figure 3 illustrates a general taxonomy of SOC estimation approaches and their relationships. Classical methods typically rely on direct current integration or voltage–SOC mappings. Model-based approaches employ equivalent circuit or electrochemical models combined with state observers such as Kalman filters. Data-driven methods use machine learning models to infer SOC directly from measured signals. Finally, hybrid frameworks integrate physical models with data-driven components to exploit the complementary strengths of both approaches.

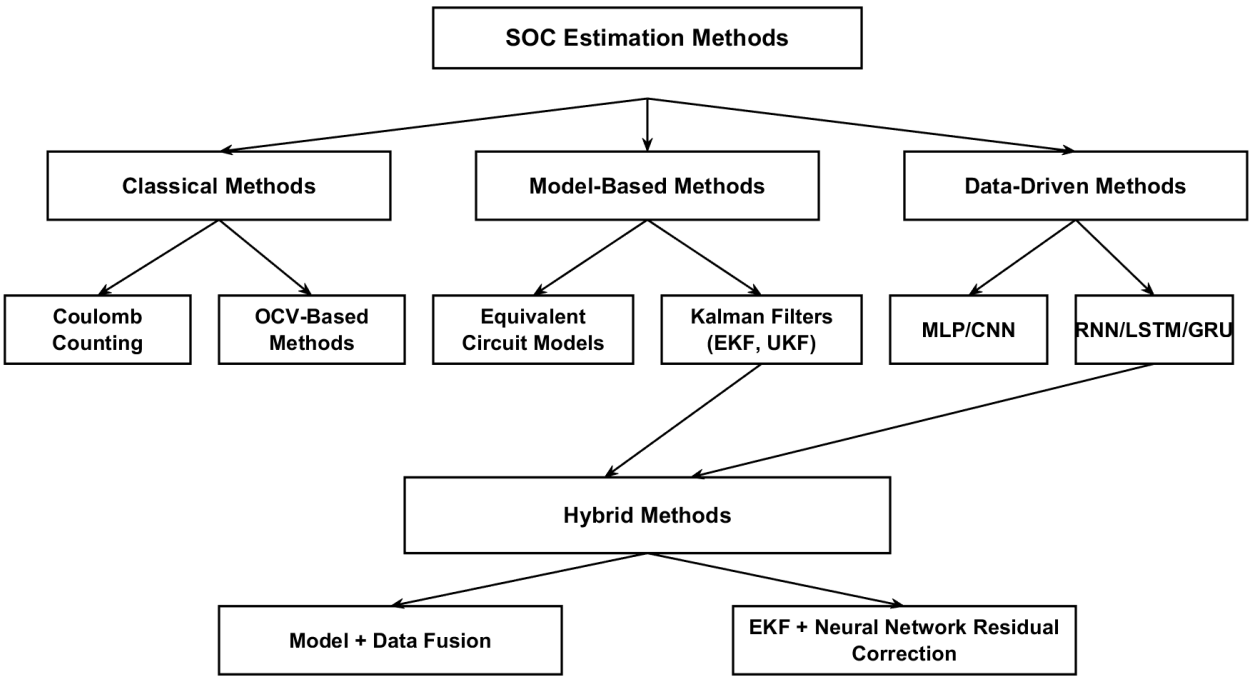

Figure 3: Taxonomy of state-of-charge (SOC) estimation methods, including classical approaches, model-based observers, data-driven methods, and hybrid frameworks.

The following subsections review these categories in greater detail.

2.3.1. Coulomb Counting

Coulomb counting, also known as the ampere-hour integration method, is one of the simplest SOC estimation techniques used in battery management systems.

The SOC is updated by integrating the measured current over time

$$SOC(t) = SOC(t_0) + (\frac{1}{Q_{nom}}) \int I(t)dt$$

The method is computationally efficient and straightforward to implement in real-time systems. However, it suffers from several important limitations: sensitivity to current measurement errors, dependence on accurate initial SOC, and accumulation of integration drift over time.

Even small sensor offsets may accumulate and lead to significant estimation errors during long-term operation [13], [26].

2.3.2. Model-Based Observer Methods

To overcome the limitations of simple integration methods, model-based observers have been widely developed. These approaches rely on equivalent circuit models (ECMs) or electrochemical models to describe battery dynamics.

Among the various observer techniques, Kalman-filter-based algorithms are the most widely adopted in practical battery management systems. The theoretical foundations of nonlinear Kalman filtering and sigma-point filtering methods are described in [3], [9], [15]. These approaches have been widely applied to lithium-ion battery SOC estimation problems.

Extended Kalman Filter

The Extended Kalman Filter (EKF) is commonly used for nonlinear SOC estimation problems. In EKF-based estimation, the battery dynamics are expressed in a nonlinear state-space representation:

$$x_{k+1} = f(x_k, u_k) + w_k$$
$$y_k = h(x_k, u_k) + v_k$$

where x_k is the state vector (e.g., SOC and polarization voltages), u_k is the input (current), y_k is the measured output (terminal voltage), w_k and v_k represent process and measurement noise, respectively.

The EKF recursively estimates the internal battery states through two main steps:

1. prediction using the system model,
2. correction using voltage measurements.

Due to its balance between computational efficiency and estimation accuracy, EKF has become a standard solution for SOC estimation in many practical BMS implementations [10], [11], [14].

However, EKF accuracy strongly depends on accurate model parameterization and voltage observability.

2.3.3. Neural Network Approaches

Several machine learning architectures have been proposed for SOC estimation. Deep neural networks and recurrent neural networks have demonstrated strong performance under dynamic load conditions [18], [19], [20]. Hybrid LSTM–Kalman filtering approaches have also been investigated to combine the advantages of physical models and data-driven learning [21]. More

recent research explores combinations of neural networks with advanced filtering techniques, including UKF and adaptive observers [27], [28], [29], [30].

Among different neural network architectures, recurrent neural networks (RNNs) are particularly suitable for time-series modeling.

Recurrent Neural Networks

Battery measurements naturally form sequential data, making RNN architectures well suited for SOC estimation tasks.

Several RNN-based models have been investigated in the literature demonstrated in Table 1:

Model	Characteristics
RNN	basic recurrent structure
LSTM	strong long-term memory capability
GRU	simplified gated recurrent architecture
CNN-RNN	hybrid spatial-temporal modeling

Table 1: Overview of RNN-based architectures used for battery state estimation.

Studies have shown that LSTM-based models can achieve improved estimation accuracy under dynamic load conditions [18], [21]. However, these architectures typically require significant computational resources.

2.4. Hybrid SOC Estimation Approaches

Purely model-based and purely data-driven methods both exhibit limitations. Model-based approaches depend on accurate parameterization, while data-driven models may suffer from poor generalization outside the training dataset.

Hybrid estimation frameworks aim to combine the advantages of both approaches. In such systems:

- a physics-based model provides the baseline estimate
- a neural network learns residual estimation errors

Several hybrid architectures have been proposed in the literature, including:

- neural-network-assisted Kalman filters
- adaptive parameter estimation using machine learning
- residual error correction networks

These approaches allow the preservation of physical interpretability while improving estimation accuracy [5], [17], [22].

2.5. Motivation for the Proposed Hybrid EKF–GRU Framework

Considering the challenges associated with SOC estimation in LFP batteries, particularly the reduced voltage observability in the OCV plateau region, hybrid estimation strategies represent a promising solution.

In this work, a hybrid estimation framework combining an Extended Kalman Filter and a recurrent neural network is proposed.

The EKF provides a physically interpretable baseline estimate based on an equivalent circuit model and voltage feedback. However, model mismatch and nonlinear battery dynamics may still produce structured residual errors.

To capture these residual patterns, a gated recurrent unit (GRU) neural network is employed as a correction layer.

Why GRU?

Among the various recurrent architectures, GRU was selected for several reasons:

- lower computational complexity than LSTM
- fewer parameters and faster training
- comparable performance for sequential modeling tasks
- suitability for real-time applications

Table 2 compares commonly used recurrent architectures.

Architecture	Parameters	Complexity	Suitability for BMS
RNN	low	limited memory	low
LSTM	high	computationally heavy	moderate
GRU	moderate	efficient	high

Table 2: Comparison of recurrent neural network architectures in terms of parameters, complexity, and suitability for battery management systems (BMS).

Because battery management systems typically operate on embedded hardware with limited computational resources, GRU offers a favorable balance between modeling capability and computational efficiency.

This motivates the development of the hybrid EKF–GRU framework presented in the following chapters.

3. SOC Estimation Framework

This section describes the experimental framework used to evaluate the proposed hybrid EKF–GRU SOC estimation method. It presents the experimental dataset used in the study, the preprocessing procedures applied to the raw measurements, and the construction of the reference SOC used for model validation. In addition, the baseline estimation approaches used for comparison with the proposed hybrid method are introduced, together with the validation protocol and performance metrics used for the quantitative assessment of the models.

The objective of this section is to ensure transparency and reproducibility of the experimental evaluation by clearly documenting the data source, preprocessing procedures, and the methodology used for model comparison.

3.1. Experimental Dataset and Preprocessing

This section introduces the experimental dataset used in this study and describes the preprocessing procedures applied prior to model development. Since the performance of the proposed SOC estimation framework strongly depends on the quality and consistency of the input data, careful preparation of the dataset is a critical step in the experimental pipeline.

First, the characteristics of the experimental dataset and the testing conditions are described. Subsequently, the preprocessing procedures applied to the raw measurements are presented, including signal validation, filtering of physically inconsistent measurements, and segmentation of the dataset into individual charge–discharge cycles. These steps ensure that the dataset is suitable for the subsequent stages of the SOC estimation framework.

3.1.1. Experimental Dataset Description

The dataset used in this study consists of experimental measurements obtained from a lithium-ion battery cell based on lithium iron phosphate (LFP) chemistry. The data correspond to a cylindrical 18650 lithium-ion cell, which is a widely used form factor in electric mobility and stationary energy storage applications.

The experiments were conducted under controlled laboratory conditions at a constant ambient temperature of 25 °C. The test campaign consists of repeated charge–discharge cycles performed over the full state-of-charge (SOC) range from 0% to 100%. Charging was carried out using a constant-current/constant-voltage (CC–CV) protocol, while the discharge process was performed at a constant current level.

During the experiments, the battery was cycled with a current magnitude of approximately 0.5C, corresponding to the charge and discharge current levels applied in the test procedure. The dataset is organized as a continuous time-series measurement, capturing the electrical behavior of the battery throughout the entire cycling experiment.

To illustrate the typical electrical behavior of the battery during a cycle, the current and voltage profiles are shown in Figure 4 and Figure 5, respectively.

Figure 4 shows the applied current as a function of the local cycle time. The charging phase begins with a constant current stage, followed by a gradual decrease in current corresponding to the constant-voltage phase. After the charging process is completed, the battery undergoes a constant-current discharge phase. The figure highlights the repeatability of the current profile across all cycles in the dataset.

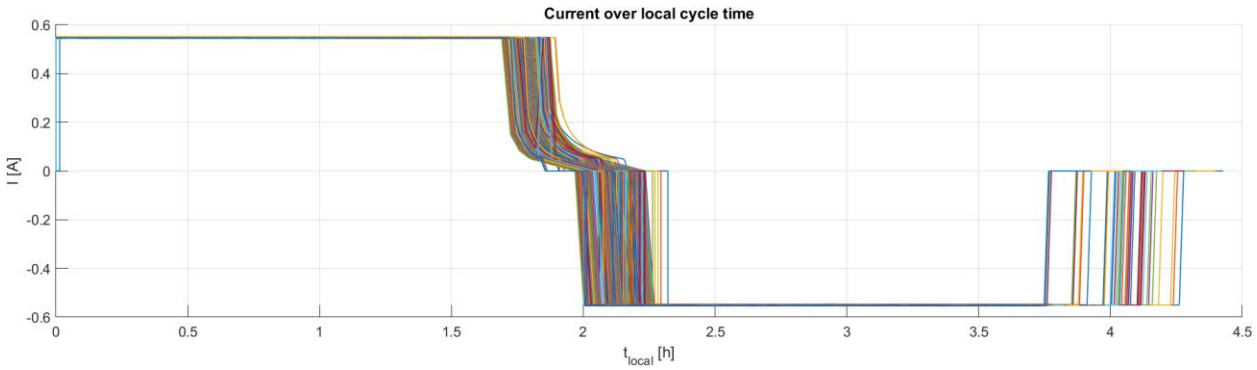

Figure 4: Current profiles of all cycles in localized cycle time.

Figure 5 shows the corresponding voltage evolution during the charge–discharge cycle. At the beginning of the charging phase, the voltage rapidly increases before entering a relatively flat region characteristic of LFP chemistry. During the discharge phase, the voltage gradually decreases until the lower cutoff voltage is reached. The consistent shape of the voltage trajectories across multiple cycles indicates stable experimental conditions during the data collection process.

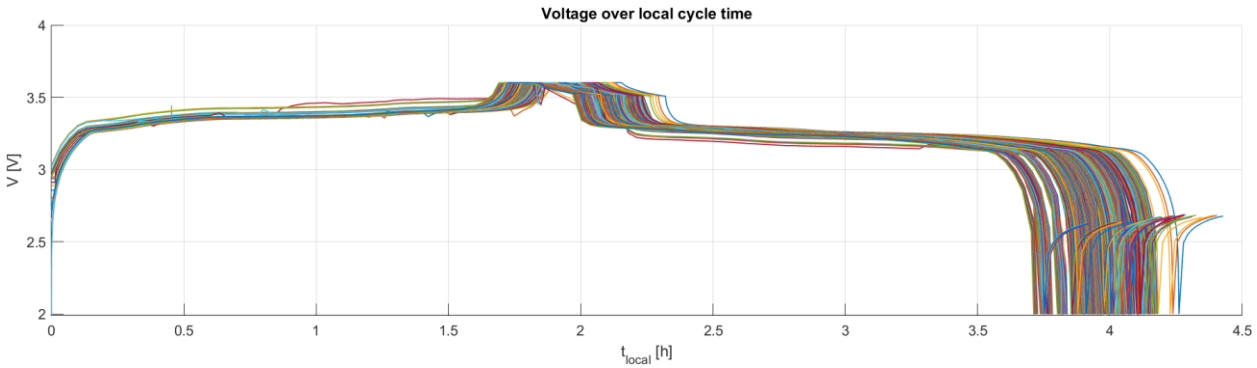

Figure 5: Voltage profiles of all cycles in localized cycle time.

The dataset provides time-series measurements recorded at each sampling step. For every measurement point, the following variables are available: the timestamp t, the applied current I, the terminal voltage V, the accumulated charged capacity Q_{chg}, and the accumulated discharged capacity Q_{dis}. In the dataset convention, positive current values correspond to charging, whereas negative values indicate discharging. The charge and discharge capacity variables represent the cumulative amount of charge transferred to and from the cell, respectively, since the beginning of the corresponding charge or discharge phase.

These measured quantities form the basis for reconstructing key internal battery states. In particular, the available current and capacity signals enable the construction and verification of the reference State of Charge (SOC) through capacity-based methods, while the evolution of the effective capacity over the cycling history allows the estimation of the State of Health (SOH). These reconstructed quantities are subsequently used as reference signals for the development, calibration, and validation of the SOC estimation framework proposed in this thesis.

The dataset is recorded as a continuous time-series signal containing multiple charge–discharge cycles. In order to prepare the dataset for algorithm development and model validation, several preprocessing steps were applied to the raw measurements. These preprocessing procedures are described in the following section.

3.1.2. Data Preprocessing

Before the dataset could be used for model development, several preprocessing steps were applied to ensure data consistency and to prepare the measurements for the subsequent SOC estimation framework. The preprocessing procedure included signal validation, physical filtering of the measurements, and segmentation of the data into individual charge–discharge cycles.

The original dataset consisted of 411,350 measurement samples, recorded as a continuous time series. Each sample contained the following variables: the measurement index (*Data_Point*),

timestamp (*t*), current (*I*), terminal voltage (*V*), cycle index (*cycle*), accumulated charged capacity (*Qchg*), and accumulated discharged capacity (*Qdis*).

The first preprocessing step consisted of verifying the numerical validity of the signals. In this step, samples containing non-finite values (e.g., NaN or Inf) were removed. However, the inspection showed that all measurements in the dataset were numerically valid, and therefore no samples were removed at this stage.

The second step involved applying physical bounds filtering in order to eliminate measurements that were outside the physically plausible operating limits of the battery. The following constraints were imposed:

- Time range: $0 \leq t \leq 5 \times 10^8$s
- Current range: $-10 \leq I \leq 10$A
- Voltage range: $1.5 < V \leq 5.0$V
- Capacity range: $0 \leq Q \leq 20$Ah

These bounds were selected to remove potential outliers while remaining significantly wider than the expected operating limits of the tested cell. After applying these constraints, 914 samples were removed, resulting in a cleaned dataset containing 410,436 samples.

A diagnostic analysis of the filtered dataset revealed that the measurements were recorded within the following operating ranges:

- Current: −0.554 A to 0.552 A
- Voltage: 1.986 V to 3.601 V
- Charged capacity: 0 to 1.099 Ah
- Discharged capacity: 0 to 1.070 Ah

These ranges are consistent with the expected operating behavior of a single 18650 lithium iron phosphate (LFP) cell cycled at approximately 0.5C.

The dataset is organized into individual charge–discharge cycles identified by the variable *cycle*. After filtering, the cycle indices ranged from 1 to 3050. The final cycle was excluded from the analysis to avoid potential issues related to incomplete measurement sequences. As a result, 3049 cycles were retained for further processing.

For the purpose of model implementation and analysis, the dataset was then segmented into individual cycles. Each cycle was extracted and stored as a separate time series. In addition to the global timestamp t_g, a local cycle time t_s was introduced for each cycle by subtracting the initial timestamp of that cycle:

$$t_s = t_g - t_g(1)$$

This transformation simplifies the interpretation of the cycle dynamics and facilitates subsequent visualization and modeling procedures.

A diagnostic evaluation of the time increments within each cycle was also performed. While the dataset generally maintains a monotonically increasing time sequence, seven cycles exhibited non-positive local time increments, indicating minor irregularities in the recorded timestamps. These irregularities were considered negligible and were therefore retained, as they do not significantly affect the SOC estimation process.

As a result of the preprocessing procedure, a cleaned and structured dataset was obtained. The processed dataset consists of a global time-series table as well as a cycle-segmented representation containing 3049 cycles. This processed dataset serves as the input for the subsequent stages of the framework, including reference SOC construction, baseline Coulomb counting estimation, and the implementation of the Extended Kalman Filter (EKF) and the hybrid neural network model.

3.2. Reference SOH and SOC Construction

After the preprocessing stage, the next step was related to building the necessary reference quantities for validating the model. More specifically, the cycle-wise actual capacity of the battery under consideration, as well as its corresponding SOH, were estimated. These quantities were necessary for building a consistent reference SOC, as it is expected that the actual capacity of the battery will change over time due to degradation phenomena.

3.2.1. Cycle-wise Capacity and SOH Estimation

Following the dataset preprocessing stage, the next step consisted of estimating the cycle-wise actual capacity of the battery and the corresponding State of Health (SOH) throughout the entire test campaign. These quantities are required for the subsequent construction of the reference SOC and for analyzing the degradation behavior of the cell over repeated cycling.

For each cycle, the actual capacity Q_{act} was defined using the discharge capacity recorded in the dataset. Specifically, the cycle capacity was obtained from the final value of the discharge capacity trace at the end of the discharge phase:

$$Q_{act} = Q_{dis}^{end}$$

This dataset-based definition was selected as the primary capacity estimation method because the discharge capacity trace directly represents the amount of charge delivered by the battery during the discharge process.

To verify the reliability of this capacity estimate, an independent Coulomb counting method was also applied. In this approach, the discharged capacity was reconstructed by integrating the measured discharge current over time:

$$Q_{act,CC} = \frac{1}{3600}\sum I_{dis}(t)\Delta t$$

where I_{dis} represents the magnitude of the discharge current and Δt denotes the sampling interval between consecutive measurements. This method provides an independent estimate of the cycle capacity based solely on current measurements.

The evolution of the cycle capacity obtained using both methods across the entire dataset is shown in Figure 6.

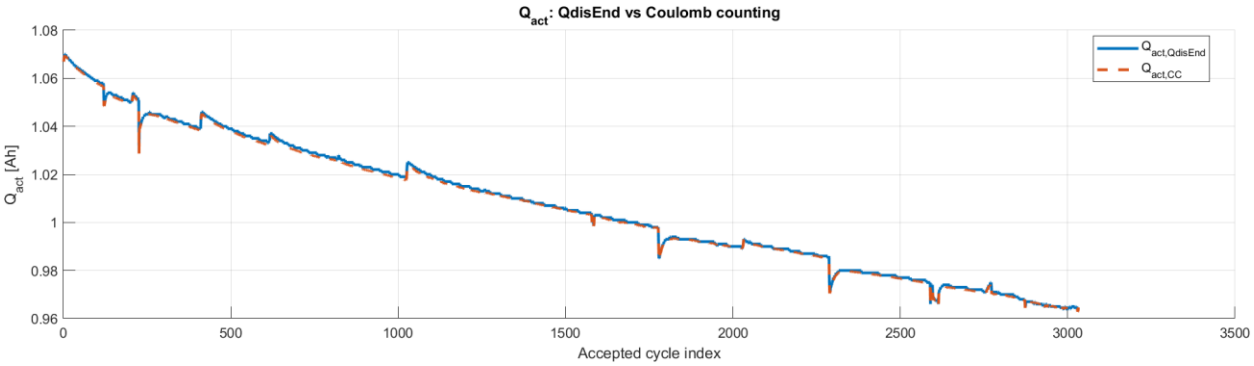

Figure 6: Comparison of estimated actual capacity Q_{act} obtained from discharge-end capacity and Coulomb counting over the accepted cycle index.

Figure 6 illustrates the capacity trend over the accepted cycle indices. Both curves follow nearly identical trajectories, indicating a gradual decrease in capacity as cycling progresses. The close overlap between the dataset-based capacity and the Coulomb counting estimate confirms the consistency of the measurements and the reliability of the capacity estimation.

To further evaluate the difference between the two estimation methods, the cycle-wise error between the Coulomb counting estimate and the dataset-based capacity was analyzed. The resulting difference is shown in Figure 7.

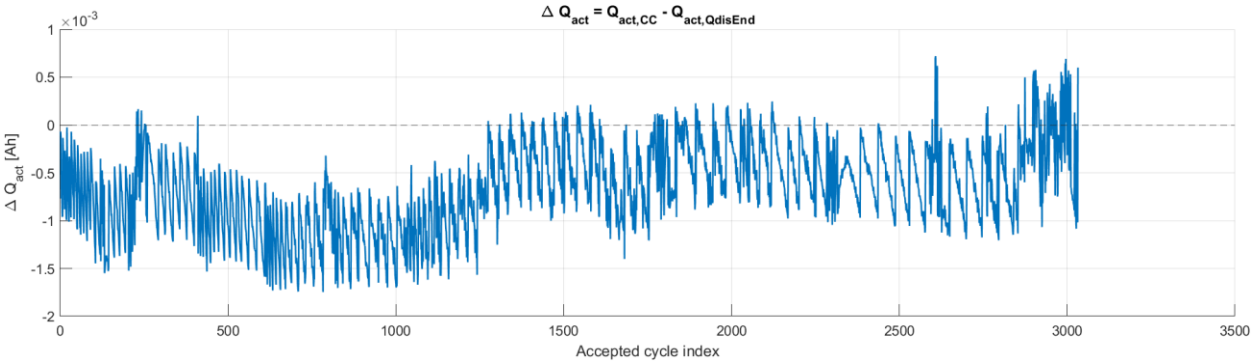

Figure 7: Capacity estimation error across accepted cycles.

As shown in Figure 7, the difference between the two capacity estimates remains very small throughout the entire test campaign, typically within the order of 10^{-3}Ah. This small deviation confirms that the dataset-based capacity trace provides an accurate representation of the discharged capacity.

Using the estimated cycle capacity, the State of Health (SOH) of the battery was computed as the ratio between the actual capacity and the nominal capacity of the cell:

$$SOH = \frac{Q_{act}}{Q_{nom}}$$

where Q_{nom} represents the nominal capacity of the battery cell.

The evolution of SOH throughout the cycling experiment is presented in Figure 8.

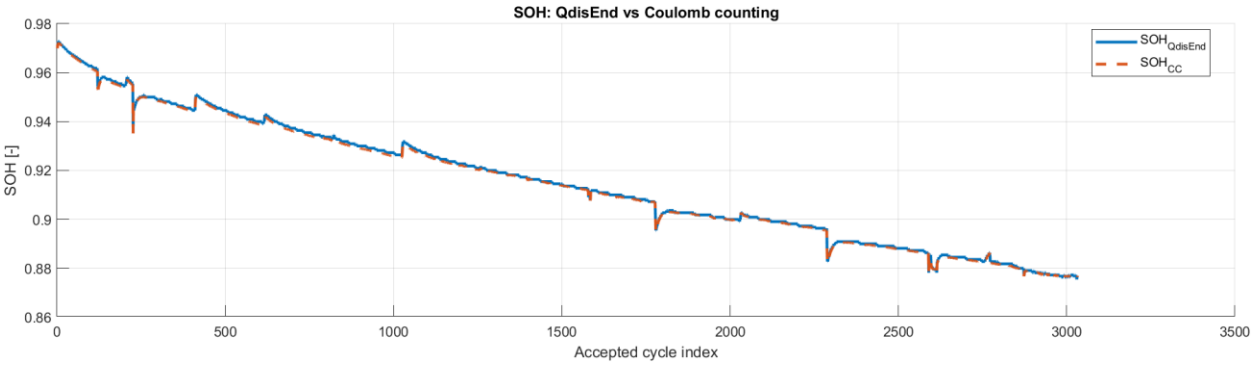

Figure 8: Comparison of SOH estimated from discharge-end capacity and Coulomb counting across accepted cycles.

Figure 8 shows a gradual decrease in SOH as the number of cycles increases, reflecting the natural capacity degradation of the battery over repeated charge–discharge cycles. As expected, the SOH values computed using both capacity estimation methods follow very similar trends.

The difference between the SOH estimates obtained from the two methods is shown in Figure 9.

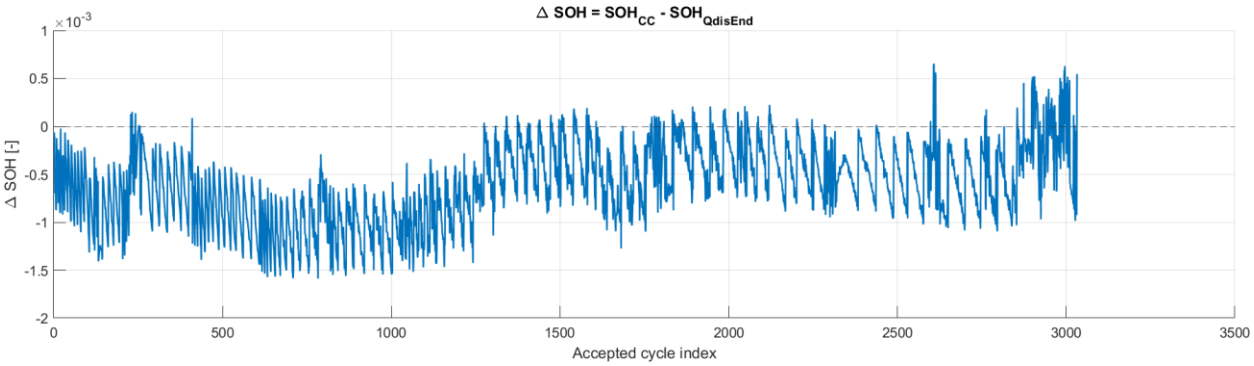

Figure 9: SOH estimation error across accepted cycles.

The deviations between the two SOH estimates remain very small and follow the same pattern observed in the capacity comparison, further confirming the consistency of the estimation procedure.

Finally, a series of cycle-quality checks were applied to ensure that only valid cycles were used for further analysis. These checks verified the presence of both charge and discharge segments and ensured that a valid capacity value could be determined for each cycle. After applying these criteria, 3041 cycles were retained and used for the subsequent stages of the SOC estimation framework.

3.2.2. Reference SOC Construction

Reliable evaluation of SOC estimation algorithms requires a well-defined reference SOC trajectory. This reference must represent the true evolution of the battery charge throughout the cycle and should not depend on the estimation algorithm that will later be validated. In addition, the reference SOC should remain consistent over the entire charge–discharge cycle and should be sufficiently robust to measurement noise and potential irregularities in the recorded signals.

To satisfy these requirements, the reference SOC used in this work was constructed using two complementary approaches. The primary reference was derived directly from the capacity measurements provided in the dataset, while an independent Coulomb counting method was used as a verification mechanism.

The primary SOC reference was defined using the measured charge and discharge capacity traces. During the charging phase, the SOC was computed from the accumulated charged capacity recorded in the dataset. Once the discharge phase begins, the SOC trajectory was reconstructed using the remaining stored charge in the cell based on the measured discharge capacity. The resulting reference SOC can therefore be expressed as

$$SOC_{ref} = \frac{Q_{eq}}{Q_{act}}$$

where Q_{eq} represents the equivalent stored charge derived from the dataset capacity measurements and Q_{act} denotes the cycle-wise actual capacity obtained in the previous section.

To verify the correctness of the constructed reference, a second SOC trajectory was calculated using the Coulomb counting method, which reconstructs SOC by integrating the measured current over time. In this case, the SOC evolution is given by

$$SOC_{ref,CC} = SOC_0 + \frac{1}{Q_{act,CC}} \int I(t)dt$$

where SOC_0 is the initial SOC of the cycle and $Q_{act,CC}$ represents the cycle capacity obtained through current integration. This approach provides an independent estimate of the SOC trajectory and allows the consistency of the capacity-based reference to be assessed.

The comparison between the two SOC trajectories for all cycles is shown in Figure 10.

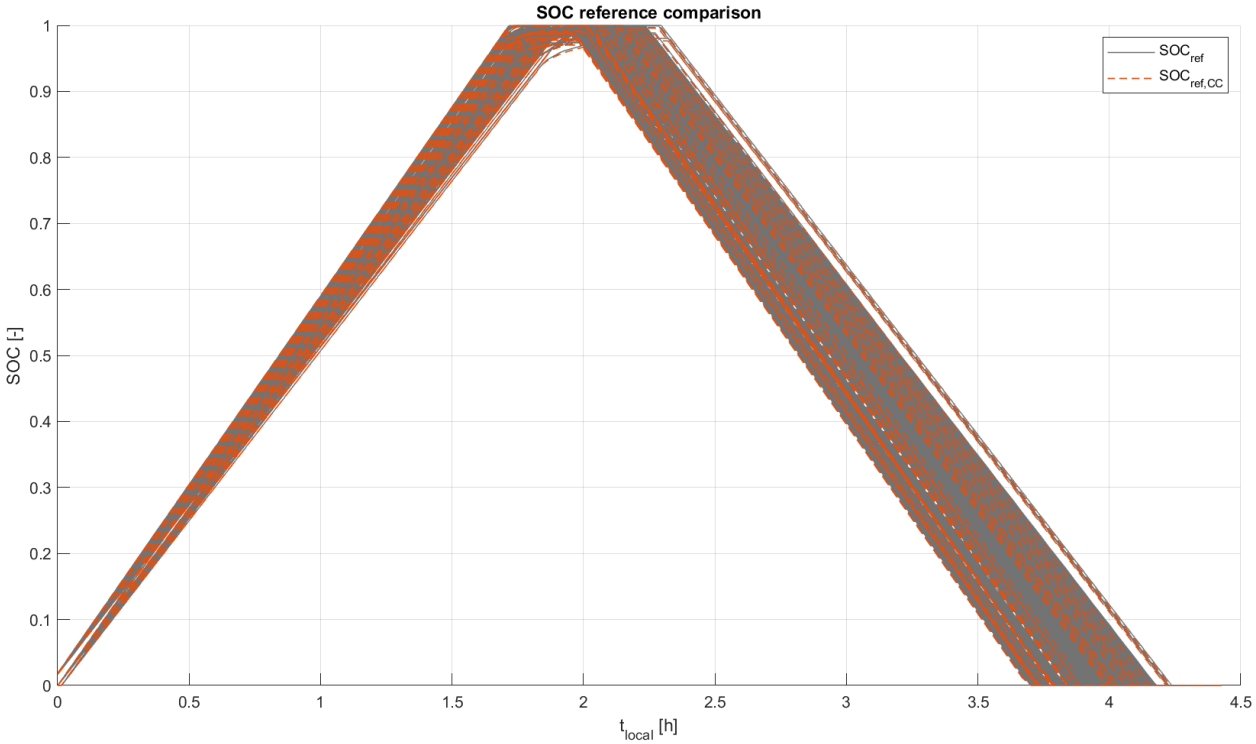

Figure 10: Comparison of reference SOC trajectories obtained from dataset capacities and Coulomb counting in local cycle time.

As illustrated in the figure, the SOC trajectories obtained from the dataset capacity measurements and from Coulomb counting follow nearly identical paths over the entire charge–discharge cycle. This close agreement confirms the reliability of the dataset-based SOC reference and validates its use as the ground truth for the subsequent SOC estimation analysis.

To further analyze the consistency of the constructed SOC reference, the relationship between the measured terminal voltage and the reference SOC was examined. The voltage–SOC characteristics obtained during the charge and discharge phases are presented in Figures 11 and 12, respectively.

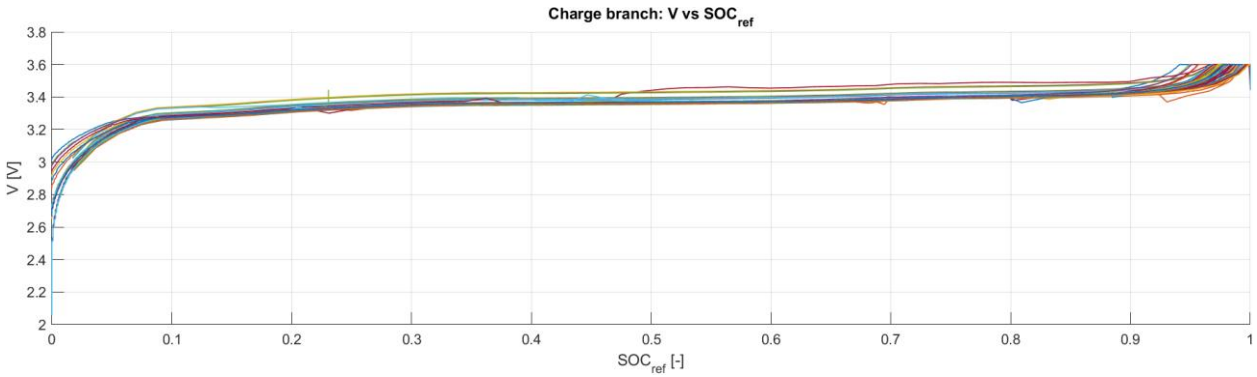

Figure 11: Voltage vs reference SOC during charge for all valid cycles.

Figure 11 shows the voltage evolution as a function of the reference SOC during the charging phase. The curves display a rapid voltage increase at low SOC values followed by a wide plateau region, which is characteristic of lithium iron phosphate cells.

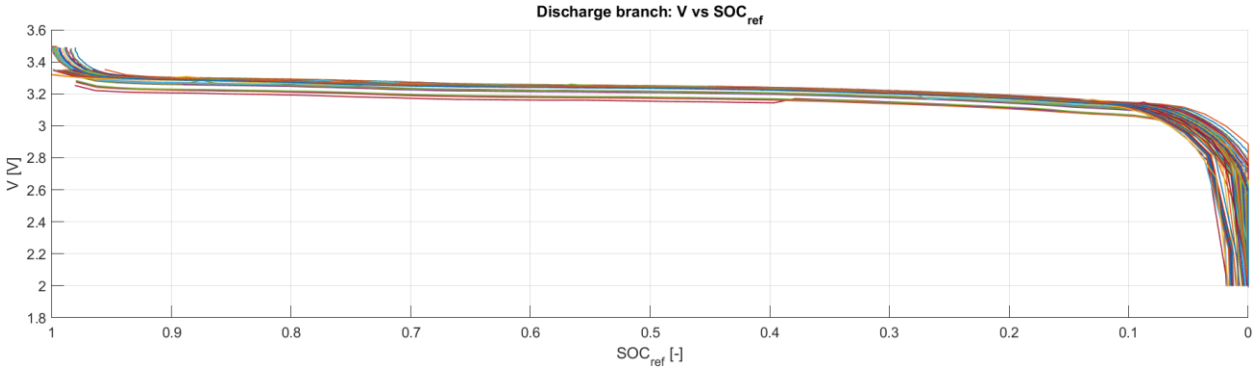

Figure 12: Voltage vs reference SOC during discharge for all valid cycles.

Figure 12 presents the voltage behavior during the discharge phase. Similarly, a relatively flat voltage plateau can be observed over a large SOC interval, followed by a sharp voltage drop near the end of discharge. The consistent shape of these curves across multiple cycles further supports the validity of the constructed SOC reference.

As a final quality control step, cycles that did not reach a sufficiently high SOC level during the charging phase were excluded from the dataset to ensure reliable normalization of the SOC trajectory. After applying this filtering criterion, 3032 cycles remained and were used for the development and validation of the SOC estimation framework presented in this thesis.

3.3. Baseline SOC Estimation

In order to evaluate the performance of the proposed hybrid SOC estimation framework, a baseline estimation method was implemented as a reference for comparison. Baseline models play an important role in experimental validation because they provide a simple and widely used benchmark against which more advanced estimation approaches can be assessed.

Among the available SOC estimation techniques, Coulomb Counting (CC) is one of the most commonly used methods in battery management systems due to its simplicity and low computational requirements. However, despite its simplicity, the method is known to suffer from several limitations, such as sensitivity to current measurement errors, accumulation of integration drift, and dependence on the knowledge of the battery capacity. For these reasons, Coulomb Counting is typically used as a baseline estimator when evaluating more advanced model-based or data-driven SOC estimation methods.

In this work, Coulomb Counting was implemented as a baseline SOC estimator in order to provide a reference performance level for the proposed hybrid EKF–GRU approach.

3.3.1. Coulomb Counting Implementation

The Coulomb Counting method estimates the state of charge by integrating the measured current over time and normalizing it by the nominal battery capacity. The SOC evolution can be expressed as

$$SOC(t) = SOC(t_0) + \frac{1}{Q_{nom}} \int_{t_0}^{t} \eta I(\tau)\, d\tau$$

where Q_{nom} represents the nominal capacity of the battery, $I(t)$ is the measured current, and η denotes the Coulombic efficiency of the charging or discharging process.

In the present implementation, the Coulomb Counting model was applied independently to each cycle of the processed dataset. The integration was performed using the measured current and the local cycle time increment. The SOC estimate was initialized at the beginning of each cycle using the corresponding reference SOC value, allowing the method to be evaluated in terms of its ability to track SOC variations during the cycle rather than its absolute initialization accuracy.

To account for potential efficiency differences between charging and discharging processes, separate efficiency parameters were included in the model. However, since the experimental dataset corresponds to controlled laboratory conditions, the Coulombic efficiencies were assumed to be ideal in this study:

$$\eta_{chg} = 1, \qquad \eta_{dis} = 1$$

Under these assumptions, the SOC update equation used in the discrete implementation becomes

$$SOC_k = SOC_{k-1} + \frac{\eta I_{k-1} \Delta t_k}{Q_{nom}}$$

where SOC_k is the estimated SOC at time step k, I_{k-1} is the measured current, and Δt_k is the time interval between two consecutive measurements.

For each cycle, the estimated SOC trajectory obtained through Coulomb Counting was compared with the previously constructed reference SOC. The estimation accuracy was evaluated using the Root Mean Square Error (RMSE) metric. In order to provide a more detailed assessment of the estimator performance, the RMSE was computed separately for the charging phase, the discharging phase, and the entire cycle.

This baseline implementation provides a simple yet informative benchmark that allows the performance improvements achieved by the proposed EKF-based and hybrid estimation approaches to be quantitatively evaluated in the subsequent sections.

3.4. Model-Based SOC Estimation

While Coulomb Counting provides a simple baseline for SOC estimation, it does not explicitly describe the electrical behavior of the battery. In practice, more reliable SOC estimation can be achieved using model-based approaches, where the battery dynamics are represented using an equivalent circuit model (ECM). These models relate the measured current and terminal voltage to the internal states of the battery and allow state estimation algorithms, such as the Extended Kalman Filter (EKF), to be applied.

A key component of model-based SOC estimation is the Open Circuit Voltage (OCV)–SOC relationship. The OCV curve represents the equilibrium voltage of the battery as a function of SOC and provides the main measurement link between the electrical model and the SOC state. In Kalman-filter-based estimation frameworks, the OCV–SOC relationship is used in the measurement equation and its derivative with respect to SOC is required for the computation of the filter Jacobian.

However, the terminal voltage measured during battery operation differs from the true open circuit voltage due to internal resistive losses and dynamic polarization effects. Therefore, before implementing the EKF estimator, it is necessary to identify an OCV–SOC relationship that accounts for these dynamic voltage components. In this work, the OCV curve was reconstructed using a Thevenin equivalent circuit model with a single RC polarization branch, which allows the dynamic voltage contributions to be separated from the measured terminal voltage.

The identified OCV model is subsequently used in the following sections for the implementation of the Thevenin ECM and the Extended Kalman Filter SOC estimator.

3.4.1. OCV Modeling

The OCV–SOC relationship was identified using a first-order Thevenin equivalent circuit model, which represents the electrical behavior of the battery using an ohmic resistance and a single RC polarization branch. In this model, the terminal voltage can be expressed as

$$V(t) = OCV(t) + R_0 I(t) + V_1(t)$$

where R_0 represents the ohmic resistance, $I(t)$ is the applied current, and $V_1(t)$ is the polarization voltage associated with the RC branch.

The dynamic behavior of the polarization voltage is described by

$$V_1(k+1) = a_k V_1(k) + b_k I(k)$$

with

$$a_k = e^{-\Delta t/\tau}, \qquad b_k = R_1(1 - a_k)$$

where R_1 and τ represent the resistance and time constant of the RC branch, respectively.

Using this model, the open circuit voltage can be reconstructed from the measured terminal voltage by removing the ohmic voltage drop and the polarization component:

$$OCV = V - R_0 I - V_1$$

For the identification procedure, the model parameters were selected as

$$R_0 = 0.02\,\Omega, \qquad R_1 = 0.018\,\Omega, \qquad \tau = 80\,s$$

with the initial polarization voltage set to $V_1(0) = 0$.

To construct the OCV–SOC relationship, the identification procedure was applied to the first ten accepted cycles of the dataset, which correspond to the initial stage of the battery life where degradation effects are minimal. Measurements with very small current magnitudes were excluded in order to avoid the influence of near-rest conditions and measurement noise. In total, 2718 discharge points and 2538 charge points were collected for the reconstruction of the OCV curves.

The reconstructed OCV–SOC relationship for both the charge and discharge branches is shown in Figure 13.

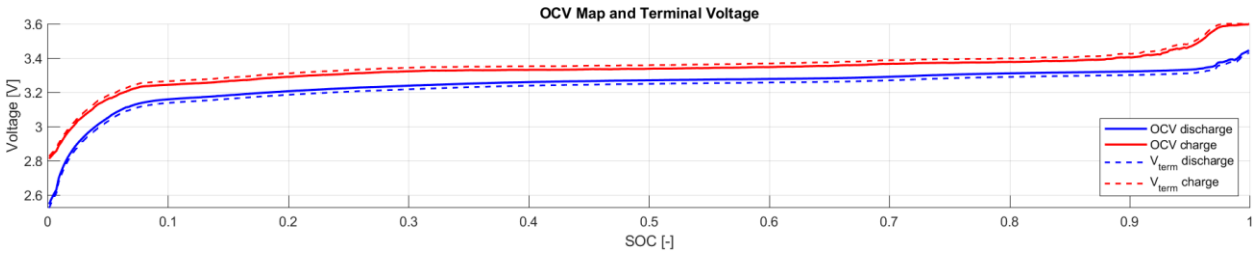

Figure 13: Charge and discharge OCV–SOC curves with corresponding terminal voltage profiles.

Figure 13 presents the reconstructed OCV curves together with the measured terminal voltage trajectories. The difference between the terminal voltage and the estimated OCV reflects the internal voltage drops caused by ohmic resistance and polarization dynamics. As expected for LFP chemistry, the OCV curve exhibits a relatively flat plateau across a wide SOC interval.

The voltage difference between the terminal voltage and the reconstructed OCV is further illustrated in Figure 14, where the deviation is plotted for both charge and discharge conditions.

$$\Delta V = V_{term} - OCV$$

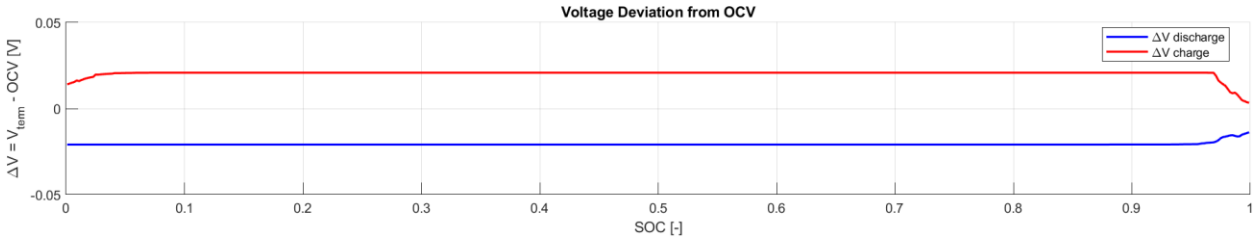

Figure 14: Voltage deviation vs. SOC during charge and discharge.

The results show that the voltage deviation remains relatively small over most of the SOC range, typically within approximately ±20 mV, indicating that the equivalent circuit model captures the dominant dynamic voltage effects of the battery.

Finally, the derivative of the OCV curve with respect to SOC was computed, as this quantity is required for the Jacobian matrix in the EKF measurement equation. The resulting derivatives for the charge and discharge branches are shown in Figure 15.

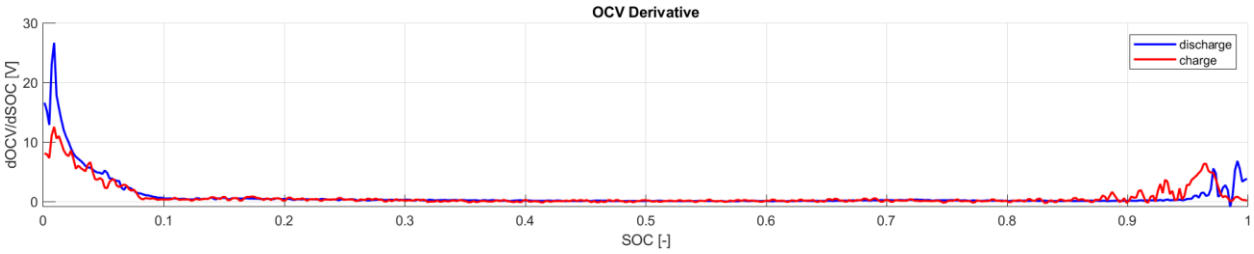

Figure 15: Derivative of the OCV–SOC relationship $dOCV/dSOC$ for charge and discharge.

The derivative curves highlight the regions where the terminal voltage is sensitive to SOC variations. In particular, the derivative becomes very small within the voltage plateau region characteristic of LFP batteries. This reduced voltage sensitivity makes SOC estimation more challenging in this region and motivates the use of advanced model-based estimation techniques such as the EKF framework presented in the following sections.

3.4.2. Thevenin Equivalent Circuit Model (ECM)

To capture the electrical dynamics of the battery during operation, a first-order Thevenin equivalent circuit model (ECM) was adopted. This model represents the battery using an open circuit voltage source combined with an ohmic resistance and a single RC polarization branch. Such a structure provides a good compromise between physical interpretability and computational simplicity, making it widely used in battery management systems and state estimation applications.

In the adopted formulation, the terminal voltage of the battery is expressed as

$$V(t) = OCV(SOC) + R_0 I(t) + V_{rc}(t)$$

where $OCV(SOC)$ represents the open circuit voltage obtained from the OCV–SOC map identified in the previous section, R_0 denotes the ohmic resistance, $I(t)$ is the applied current, and V_{rc} is the polarization voltage associated with the RC branch.

The dynamics of the polarization voltage are described by

$$V_{rc}(k+1) = a\, V_{rc}(k) + (1-a)R_1 I(k)$$

where

$$a = e^{-\Delta t/\tau}$$

and R_1 and τ represent the resistance and time constant of the polarization branch, respectively.

The model therefore contains two internal states:

$$x = \begin{bmatrix} SOC \\ V_{rc} \end{bmatrix}$$

where SOC describes the battery state of charge and V_{rc} represents the dynamic voltage drop caused by polarization effects.

The SOC state evolves according to the Coulomb counting relationship

$$SOC_{k+1} = SOC_k + \eta \frac{I_k \Delta t}{Q_{nom}}$$

where Q_{nom} is the nominal battery capacity and η is the Coulombic efficiency. In this work, both charging and discharging efficiencies were assumed equal to unity.

The parameters used for the ECM are summarized below:

$$R_0 = 0.02\,\Omega, \qquad R_1 = 0.018\,\Omega, \qquad \tau = 80\,s$$

These parameters are consistent with those used during the OCV identification stage, ensuring model consistency throughout the estimation framework.

Using this model, the predicted terminal voltage can be computed at each time step as

$$\hat{V} = OCV(SOC) + R_0 I + V_{rc}$$

The difference between the measured and predicted voltages defines the voltage residual, which is used by the EKF algorithm to correct the state estimate.

Figure 16 illustrates the voltage residual between the measured terminal voltage and the voltage predicted by the ECM.

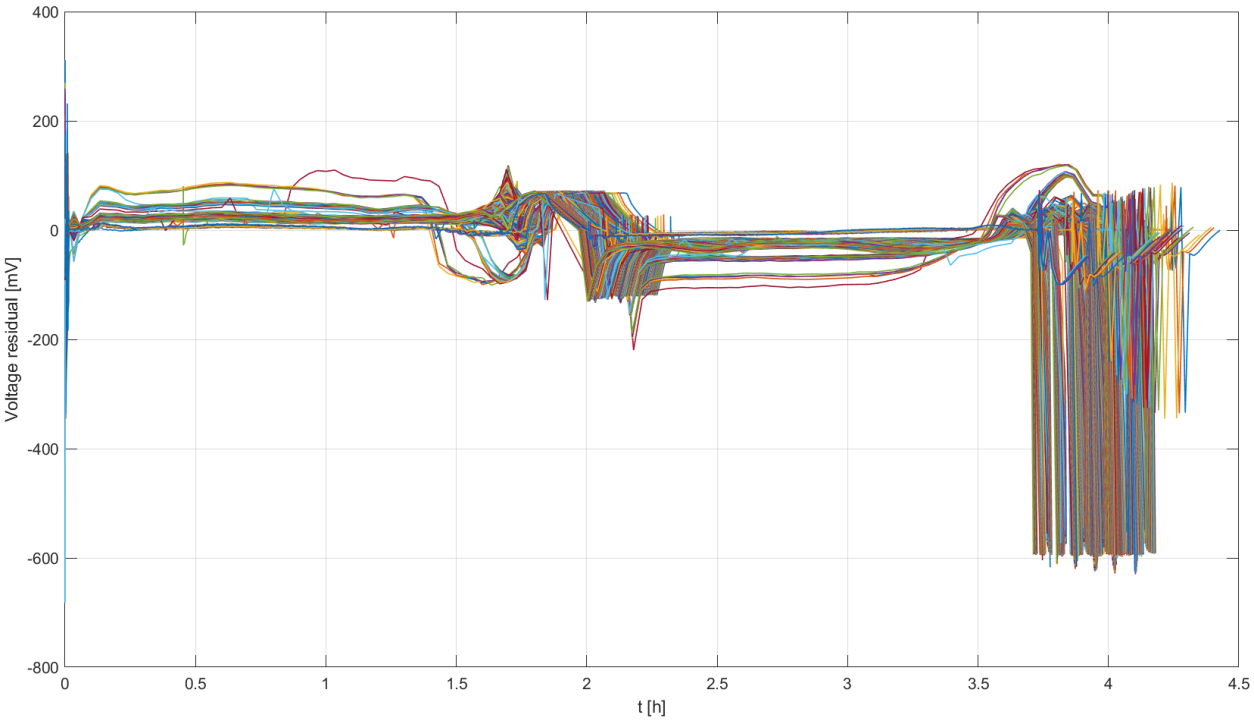

Figure 16: Overlay of voltage residuals for all cycles in local cycle time.

The figure shows that the majority of residual values remain within a relatively narrow range, indicating that the ECM captures the dominant electrical dynamics of the battery. Larger deviations occur primarily during transient events such as transitions between charging and discharging phases.

3.4.3. Extended Kalman Filter (EKF) Formulation

Based on the previously described ECM, an Extended Kalman Filter (EKF) was implemented to estimate the battery SOC during operation. The EKF is well suited for nonlinear systems such as battery models because it allows recursive state estimation while accounting for measurement noise and model uncertainty.

The EKF uses the ECM as the process model and the terminal voltage measurement as the observation. The system state vector is defined as

$$x = \begin{bmatrix} SOC \\ V_{rc} \end{bmatrix}$$

The state prediction step is obtained directly from the ECM equations:

$$SOC_{k+1} = SOC_k + \eta \frac{I_k \Delta t}{Q_{nom}}$$

$$V_{rc,k+1} = aV_{rc,k} + (1 - a)R_1 I_k$$

The measurement equation relates the predicted states to the measured terminal voltage:

$$V_k = OCV(SOC_k) + R_0 I_k + V_{rc,k}$$

Since the OCV–SOC relationship is nonlinear, the EKF linearizes the measurement equation around the current state estimate using the derivative of the OCV curve:

$$H = \begin{bmatrix} \frac{dOCV}{dSOC} & 1 \end{bmatrix}$$

The derivative $dOCV/dSOC$ is obtained from the interpolated OCV curves constructed in Section 3.4.1.

The filter uses the covariance matrices

$$Q_k = \begin{bmatrix} 10^{-5} & 0 \\ 0 & 5 \times 10^{-5} \end{bmatrix}$$

for the process noise and

$$R_k = (0.020)^2$$

for the measurement noise variance.

The initial covariance matrix was defined as

$$P_0 = \begin{bmatrix} 0.1^2 & 0 \\ 0 & 10^{-4} \end{bmatrix}$$

while the initial polarization voltage was assumed to be zero.

To smoothly transition between the charge and discharge OCV branches, a current-dependent blending function was applied using a hyperbolic tangent formulation controlled by the parameter $I_s = 1.0$. This approach avoids discontinuities in the OCV model during current sign changes.

Figure 17 shows the Kalman gain associated with the SOC state during the estimation process.

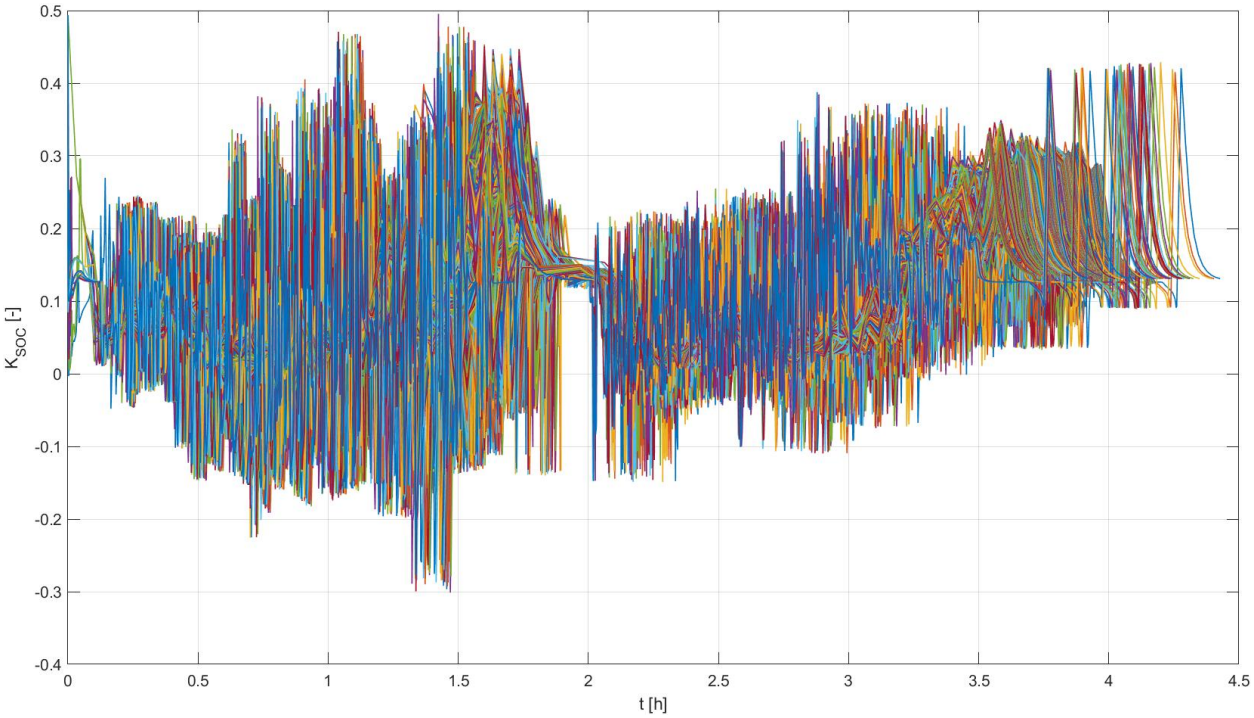

Figure 17: Kalman gain for SOC estimation across all cycles in local cycle time.

The Kalman gain determines the relative influence of the voltage measurement on the SOC correction. As expected, the gain varies significantly depending on the operating conditions and the sensitivity of the OCV curve.

Figure 18 presents the derivative of the OCV curve evaluated during the EKF operation.

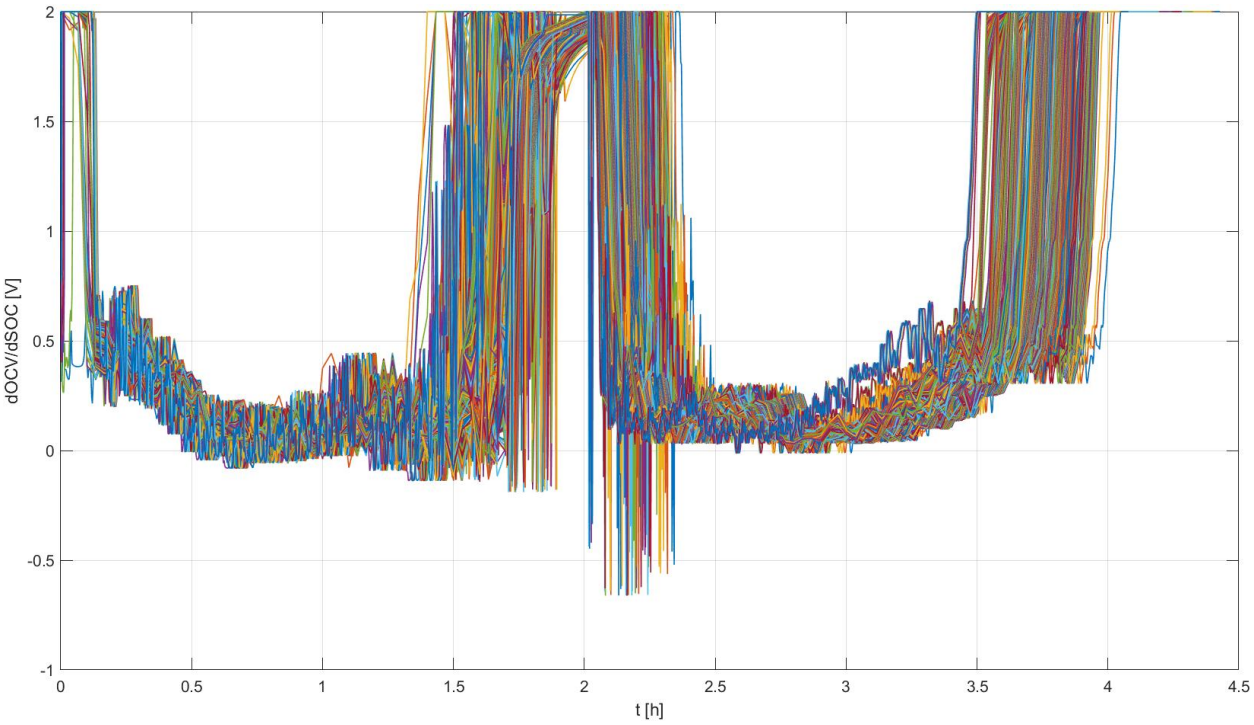

Figure 18: $dOCV/dSOC$ used in the EKF measurement model across all cycles in local cycle time.

The derivative becomes very small in the plateau region characteristic of LFP chemistry. In these regions, the terminal voltage provides limited information about SOC, which reduces the observability of the state and results in smaller correction gains.

Overall, the implemented EKF model demonstrated a mean voltage prediction bias of −4.75 mV, indicating a good agreement between the ECM prediction and the measured terminal voltage.

This model-based estimation framework serves as the main reference estimator in this work and provides the foundation for the hybrid estimation approach introduced in the subsequent sections.

3.5. Proposed Hybrid EKF–Neural Network Framework

Although the EKF provides a physically consistent estimate of SOC, its accuracy is still limited by the assumptions of the equivalent circuit model, by uncertainty in the selected parameters, and by the reduced voltage sensitivity that characterizes LFP cells over a large portion of the SOC range. For this reason, a hybrid estimation framework was developed in order to improve the EKF prediction without discarding its model-based structure.

The main idea of the proposed approach is to use the EKF as the primary estimator and then apply a data-driven correction layer based on a recurrent neural network. In this way, the neural network is not required to learn the full SOC trajectory from scratch. Instead, it learns only the residual error that remains after the EKF estimation. This residual-learning strategy is advantageous because the dominant battery dynamics are already captured by the physical model, while the neural network is used to compensate for nonlinear effects and modeling inaccuracies that are not fully represented by the ECM.

From a methodological point of view, this hybrid structure preserves the interpretability and physical consistency of the model-based estimator while exploiting the flexibility of deep learning to improve the final accuracy.

3.5.1. Hybrid Estimation Principle

The proposed framework is based on the assumption that the EKF estimate already provides a good approximation of the true SOC, and that the remaining estimation error is easier to learn than the complete SOC evolution. For this reason, the neural network was trained to predict the difference between the reference SOC and the EKF estimate:

$$\Delta SOC = SOC_{ref} - SOC_{EKF}$$

The final corrected SOC estimate of the hybrid framework is then obtained as

$$SOC_{HYB} = SOC_{EKF} + \widehat{\Delta SOC}$$

where $\widehat{\Delta SOC}$ is the correction term predicted by the neural network.

This formulation allows the model-based estimator and the neural network to play complementary roles. The EKF provides the main state trajectory based on physical equations, whereas the neural network acts as an error compensator operating on top of the EKF output.

3.5.2. Input Features and Target Definition

For each accepted cycle, the neural network was trained using sequential data derived from the reference dataset and from the EKF output. The target variable was defined as the residual SOC error between the reference and the EKF estimate.

In the final selected configuration, the following input features were used at each time step:

- EKF-based SOC estimate, SOC_{EKF}
- measured terminal voltage, V
- measured current, I
- estimated polarization voltage, V_{rc}

Thus, the input vector can be written as

$$u_k = \begin{bmatrix} SOC_{EKF,k} \\ V_k \\ I_k \\ V_{rc,k} \end{bmatrix}$$

These features were selected because they provide complementary information about the battery state and the EKF behavior. The estimated SOC represents the current model-based approximation, the voltage and current describe the instantaneous electrical operating condition, and the polarization voltage provides information about the dynamic response captured by the Thevenin model.

The target sequence used for training was defined as

$$y_k = SOC_{ref,k} - SOC_{EKF,k}$$

which corresponds to the residual SOC correction that the network must learn.

The implemented framework also supports the use of additional features, such as SOH, time increment, and signal derivatives, but these variables were not included in the final model in order to keep the feature set compact and focused on the variables most directly linked to the EKF residual.

3.5.3. GRU-Based Neural Network Architecture

Since the SOC correction problem is inherently sequential, a Gated Recurrent Unit (GRU) network was selected. Recurrent neural networks are particularly suitable for battery state estimation because they are able to exploit temporal dependencies and memory effects within charge–discharge sequences.

The final network architecture used in this work consists of:

1. a sequence input layer,
2. a GRU layer with 40 hidden units,
3. a fully connected layer with 32 neurons,
4. a ReLU activation layer,
5. a final fully connected output layer,
6. a regression layer.

This structure allows the network to process the entire cycle as a sequence and to predict a correction value at each time step. The GRU layer extracts temporal patterns from the EKF residual behavior, while the fully connected layers map the learned recurrent representation to the final correction output.

Compared with a fully data-driven direct SOC predictor, this architecture is simpler and more stable, because it only learns the residual correction signal rather than the complete SOC trajectory.

3.5.4. Training, Validation and Test Split Strategy

To evaluate the generalization capability of the neural network in a meaningful way, the cycles were not split randomly. Instead, a band-based lifecycle split strategy was adopted. This choice was motivated by the fact that battery behavior changes over life due to degradation, and a purely random split may lead to overly optimistic results if train and test samples are drawn from nearly identical regions of the lifecycle.

The accepted cycles were divided into three lifecycle bands, and within each band the following proportions were used:

$$p_{train} = 0.30, \qquad p_{val} = 0.10, \qquad p_{test} = 0.60$$

This resulted in the following split:

- 909 training cycles
- 303 validation cycles
- 1820 test cycles

The adopted split is intentionally demanding, since the majority of the data was reserved for testing. This makes the evaluation more rigorous and provides a better indication of how well the hybrid model generalizes over different stages of battery life.

3.5.5. Feature Normalization and Training Procedure

Before training, all input features were normalized using the mean and standard deviation computed exclusively from the training set. This avoids information leakage from the validation and test sets and ensures a fair evaluation of the model. Each feature was normalized according to

$$\tilde{x} = \frac{x - \mu}{\sigma}$$

where μ and σ denote the training-set mean and standard deviation of the corresponding feature.

The network was trained using the Adam optimizer with the following hyperparameters:

- learning rate: 10^{-3}
- mini-batch size: 8
- maximum number of epochs: 20

The training process was performed using a single CPU. Validation was carried out every 50 iterations in order to monitor generalization during training.

In the final selected configuration, the optional clipping of the predicted correction signal was disabled. This means that the neural network output was not artificially constrained during inference, allowing the network to learn the residual correction freely.

3.5.6. Training Behavior and Convergence

The training history of the GRU network is shown in Figure 19.

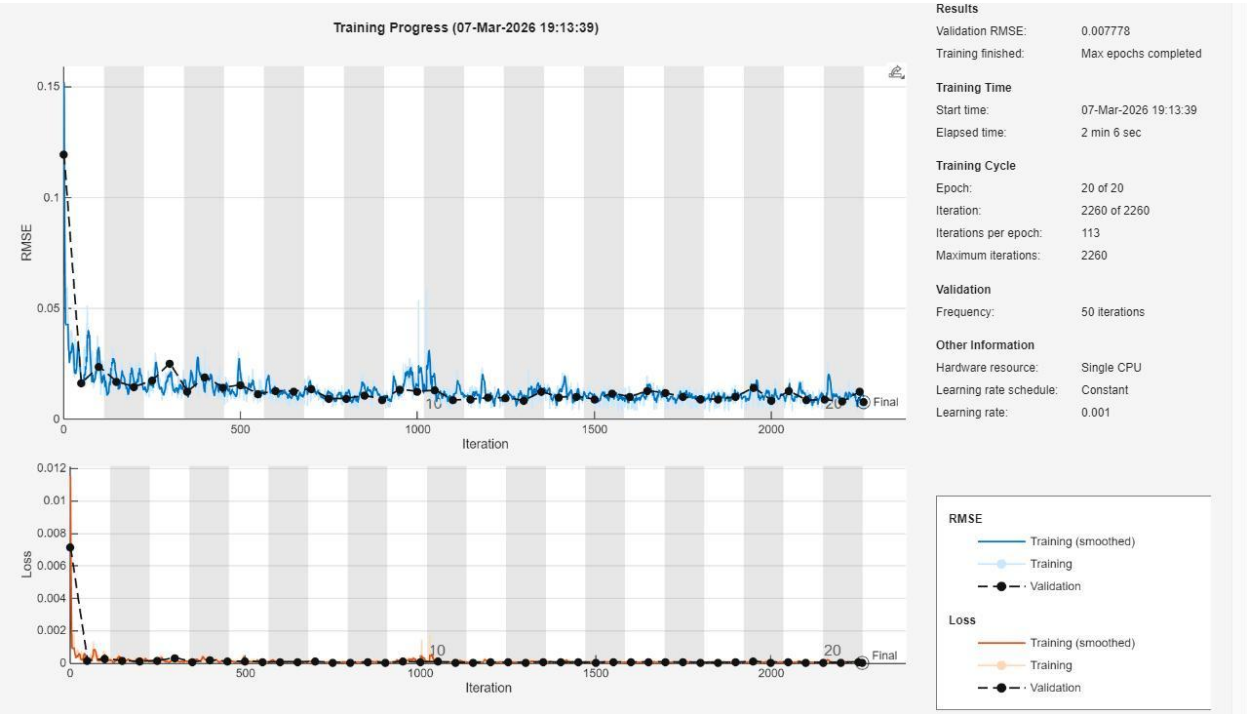

Figure 19: GRU training progress showing RMSE and loss during model training.

Figure 19 presents the evolution of the RMSE and loss during training and validation. A rapid reduction of the error can be observed during the initial iterations, followed by a more gradual stabilization phase. This behavior indicates that the main residual structure is learned quickly, while later epochs provide incremental refinement of the model.

At the end of training, the model reached a validation RMSE of 0.00778, and the training process terminated after completing the maximum number of epochs. The total training time was approximately 2 minutes and 6 seconds for 20 epochs and 2260 iterations.

The training and validation curves remain close throughout the optimization process, without signs of severe divergence. This suggests that the selected architecture and feature set provide a stable learning process and that the model does not exhibit strong overfitting under the adopted split configuration. At the same time, the remaining oscillations in the validation curve are consistent with the variability expected from cycle-to-cycle battery behavior and from the relatively demanding lifecycle-based split.

3.5.7. Hybrid SOC Reconstruction

Once the neural network predicts the residual correction sequence $\widehat{\Delta SOC}$, the final hybrid SOC estimate is reconstructed by adding the correction to the EKF estimate:

$$SOC_{HYB,k} = SOC_{EKF,k} + \widehat{\Delta SOC}_k$$

To ensure physical consistency of the prediction, the corrected SOC is bounded within the admissible interval:

$$0 \leq SOC_{HYB} \leq 1$$

This constraint prevents the estimator from producing physically infeasible SOC values.

The performance of the hybrid framework was evaluated on the test cycles by comparing the corrected SOC trajectory with the reference SOC. As in the previous sections, the evaluation was carried out separately for the charging phase, the discharging phase, and the full cycle. The root mean square error (RMSE) was used as the main accuracy metric.

The hybrid estimator combines the advantages of model-based and data-driven approaches. The EKF provides a physically grounded estimate of the SOC based on the equivalent circuit model, while the GRU network learns the residual estimation error that remains after the model-based estimation stage. By correcting the EKF trajectory rather than replacing it, the hybrid framework preserves the interpretability of the physical model while improving estimation accuracy.

The effectiveness of the proposed hybrid approach is evaluated in the next chapter through a comparative analysis of three estimators: the Coulomb Counting baseline, the model-based EKF, and the proposed hybrid EKF–GRU estimator.

4. Experimental Validation and Performance Evaluation

This chapter presents the quantitative evaluation of the proposed SOC estimation framework. The objective of this section is to assess the accuracy of the different estimation approaches introduced in Chapter 3 and to compare their performance under the experimental dataset described previously.

The evaluation is conducted progressively, starting from the baseline Coulomb Counting estimator, followed by the model-based Extended Kalman Filter (EKF), and finally the proposed hybrid EKF–Neural Network framework. This progressive structure allows a clear assessment of how each methodological component contributes to improving the SOC estimation accuracy.

To ensure a consistent and reproducible comparison, the same dataset, preprocessing pipeline, and validation protocol are applied to all estimation methods. The evaluation focuses on both charge and discharge phases, as well as on the overall cycle behavior, since the estimation difficulty and error characteristics may differ between these operating conditions.

Before presenting the individual results for each estimation method, the evaluation methodology and the adopted validation protocol are described.

4.1. Evaluation Methodology

The evaluation methodology defines how the accuracy of the SOC estimation algorithms is assessed and compared. Since the objective of this work is to quantify the improvement achieved by the proposed hybrid framework, a consistent set of performance metrics and a unified validation protocol were applied to all considered estimation methods.

The evaluation was performed using the experimentally derived reference SOC described in Chapter 3. For each estimation method, the predicted SOC trajectory was compared with the reference SOC across the available charge–discharge cycles. The comparison was carried out separately for the charge phase, the discharge phase, and the full cycle in order to capture potential differences in estimation performance between these operating conditions.

In addition to the definition of the error metrics, the validation strategy also plays a critical role in assessing the generalization capability of the proposed framework. For this reason, the evaluation protocol was designed to account for the lifecycle evolution of the battery dataset and to avoid biased results that could arise from purely random data splits.

4.1.1. Performance Metrics

The accuracy of the SOC estimation methods was quantified using the Root Mean Square Error (RMSE) between the estimated SOC and the reference SOC. The RMSE is widely used in battery management research because it provides a clear measure of the average estimation deviation while penalizing larger errors.

The RMSE is defined as

$$RMSE = \sqrt{\frac{1}{N}\sum_{k=1}^{N}\left(SOC_{est,k} - SOC_{ref,k}\right)^2}$$

Where $SOC_{est,k}$ represents the estimated SOC at sample k, $SOC_{ref,k}$ denotes the reference SOC value, and N is the total number of samples considered in the evaluation.

In order to provide a more detailed analysis of the estimator behavior, the RMSE was computed separately for different operating phases:

- Charge RMSE, calculated using samples corresponding to positive current values
- Discharge RMSE, calculated using samples corresponding to negative current values
- Overall RMSE, calculated using all valid samples within the cycle

This separation is particularly relevant for lithium iron phosphate (LFP) batteries because the voltage response and observability characteristics differ between the charge and discharge processes. By evaluating the error in each phase independently, it becomes possible to better understand how the estimation methods behave under different operating conditions.

For easier interpretation, the RMSE values are reported both in normalized SOC units and in percentage of SOC.

4.1.2. Validation Protocol

To ensure a fair and reproducible comparison between the different estimation approaches, a consistent validation protocol was applied throughout the experimental evaluation.

The dataset contains a large number of sequential charge–discharge cycles recorded over the lifetime of the tested battery cell. Since battery behavior evolves over time due to degradation effects, the data were not split randomly. Instead, a lifecycle-aware validation strategy was adopted.

The available cycles were divided into multiple lifecycle bands representing different regions of battery operation. Within each band, the cycles were partitioned into training, validation, and test subsets according to predefined proportions. This approach ensures that all subsets contain samples from different stages of the battery lifecycle and avoids the risk of evaluating the model only on cycles that are statistically similar to the training data.

The same dataset partitioning and evaluation procedure were used for all estimation methods in order to maintain consistency in the comparison. The training subset was used only for methods requiring parameter learning, while the validation subset was used to monitor model behavior during training. The final performance evaluation was carried out exclusively on the test subset.

This validation strategy provides a more reliable assessment of the estimation performance and allows the comparison between the baseline, model-based, and hybrid approaches under consistent conditions.

4.2. Baseline SOC Estimation Results

In order to establish a reference point for the evaluation of more advanced estimation techniques, a baseline SOC estimation method was first implemented using the classical Coulomb Counting (CC) approach. Coulomb Counting represents one of the most widely used SOC estimation techniques in battery management systems due to its conceptual simplicity and low computational cost. The method estimates the SOC by integrating the measured current over time, starting from a known initial SOC value.

Despite its simplicity, Coulomb Counting is sensitive to measurement noise, current integration errors, and inaccuracies in the battery capacity estimation. These limitations may lead to cumulative estimation errors over long cycling experiments, especially when the battery capacity gradually changes due to degradation. For this reason, the CC estimator serves as a useful baseline for comparison, highlighting the need for more advanced estimation methods such as model-based observers and hybrid approaches.

The performance of the Coulomb Counting estimator was evaluated by comparing the estimated SOC trajectories with the reference SOC constructed from the experimental dataset. The error metrics defined in Section 4.1 were computed for each cycle and then averaged across all available cycles.

4.2.1. Coulomb Counting Estimation Performance

The estimation accuracy of the Coulomb Counting method was first analyzed by examining the RMSE evolution across the cycling experiment. Figure 20 shows the RMSE values computed for the charging phase, the discharging phase, and the overall cycle as a function of the cycle index.

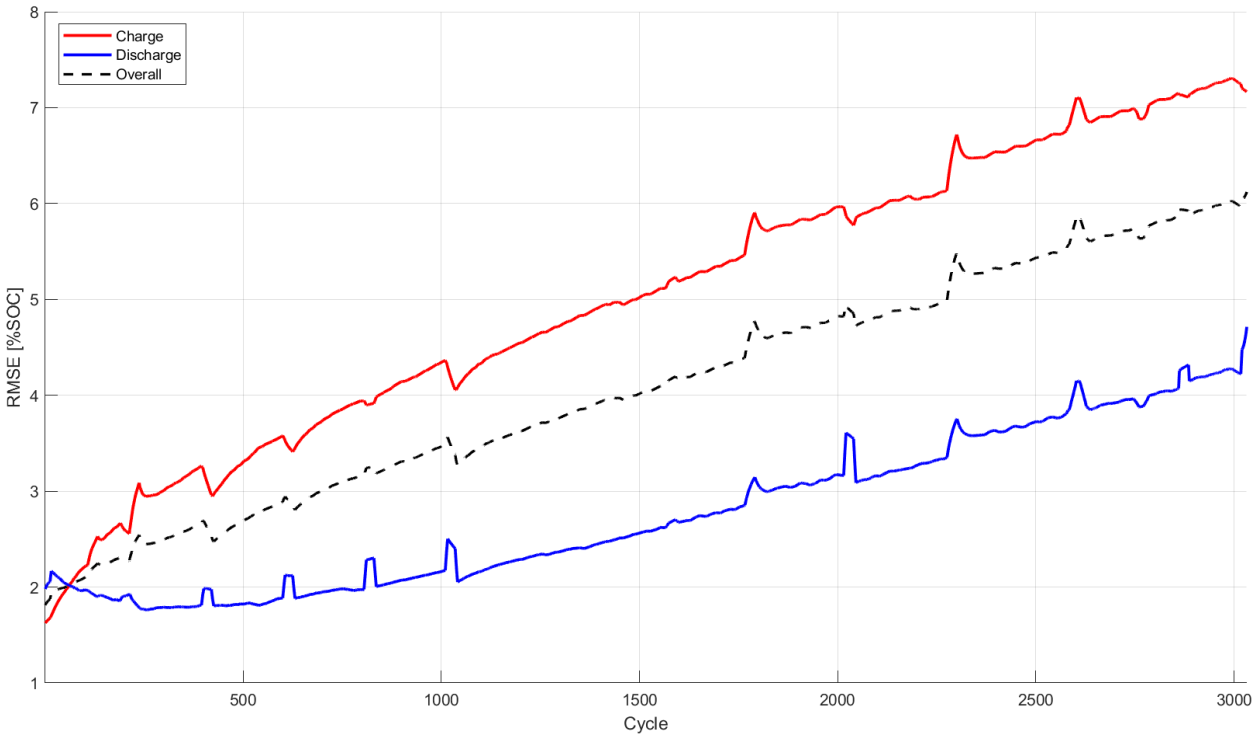

Figure 20: RMSE evolution of the Coulomb counting SOC estimator across cycles.

The results reveal a clear increase in estimation error as the number of cycles grows. In particular, the RMSE during the charging phase exhibits the largest error growth, increasing progressively over the lifetime of the dataset. This behavior is mainly associated with the cumulative integration error of the current signal and the gradual mismatch between the assumed nominal capacity and the actual battery capacity as the cell ages.

In contrast, the discharge RMSE remains significantly lower than the charge RMSE throughout the cycling experiment. This asymmetry can be attributed to the different current profiles and operating conditions between the charging and discharging phases, as well as the influence of the constant-voltage stage during charging, which may introduce additional uncertainty in the integrated charge calculation.

Overall, the RMSE trend highlights the intrinsic limitations of the Coulomb Counting approach when applied over long experimental datasets without periodic recalibration.

The average RMSE values obtained for the CC estimator across all cycles are summarized below:

- Charge RMSE: 0.0501 (5.01 %SOC)
- Discharge RMSE: 0.0277 (2.77 %SOC)
- Overall RMSE: 0.0409 (4.09 %SOC)

These values confirm that the Coulomb Counting method provides only a moderate level of accuracy under the considered experimental conditions. While the method can track the general SOC evolution, the accumulated error becomes significant over extended cycling.

To further illustrate the behavior of the CC estimator, Figure 21 presents example SOC trajectories for three representative cycles taken from different stages of the dataset.

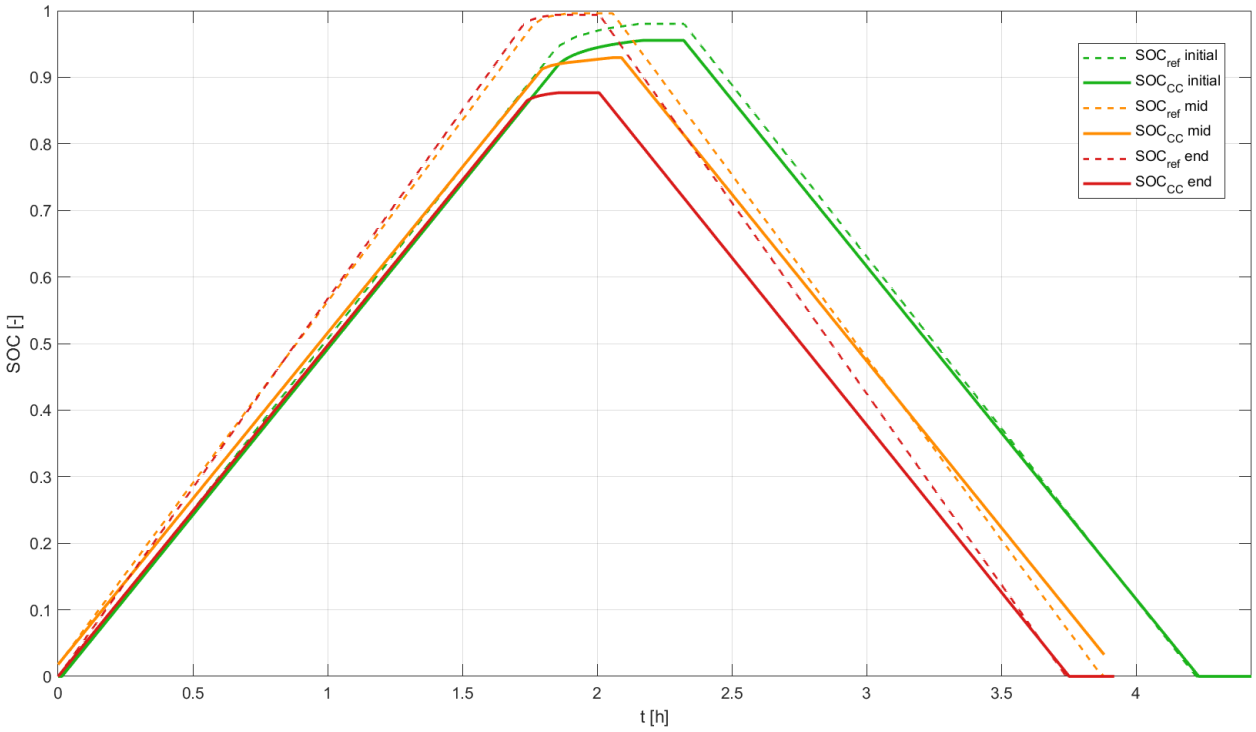

Figure 21: Comparison of reference SOC and Coulomb counting SOC estimation for representative cycles.

The figure shows the SOC trajectories for an early cycle, an intermediate cycle, and a late-life cycle. For the first cycle, the CC estimator closely follows the reference SOC, indicating that the initial estimation conditions are relatively accurate. However, as the cycle index increases, the discrepancy between the estimated SOC and the reference SOC becomes more pronounced.

In the later cycles, the CC estimator increasingly underestimates the SOC during the charging phase and deviates more strongly during the discharge process. This progressive deviation is

consistent with the RMSE trends observed in Figure 20 and reflects the cumulative integration error inherent to the Coulomb Counting method.

These observations confirm that while Coulomb Counting provides a useful baseline estimator, its accuracy is limited when applied over long-term cycling data without correction mechanisms. Consequently, more advanced estimation approaches are required to compensate for these accumulated errors and to improve the robustness of SOC estimation under real operating conditions.

The next section therefore investigates the performance of a model-based SOC estimator based on the Extended Kalman Filter (EKF), which incorporates the battery voltage response through an equivalent circuit model.

4.3. EKF-Based SOC Estimation Results

Following the evaluation of the baseline Coulomb Counting estimator, the performance of the model-based SOC estimation approach was investigated using the Extended Kalman Filter (EKF) described in Chapter 3. Unlike Coulomb Counting, which relies solely on current integration, the EKF incorporates both current and voltage measurements through the equivalent circuit model of the battery. This allows the estimator to correct the SOC prediction using the measured voltage response, thereby reducing the cumulative error that typically affects current-integration-based methods.

The EKF estimator was implemented using the Thevenin equivalent circuit model introduced earlier, combined with the OCV–SOC relationship derived from the experimental dataset. The state vector of the estimator consisted of the SOC and the polarization voltage associated with the RC branch of the model. By continuously updating these states based on the measured terminal voltage, the EKF provides a dynamic correction mechanism that improves the robustness of the SOC estimation.

The performance of the EKF estimator was evaluated using the same dataset and validation protocol described in Section 4.1. In particular, the estimation accuracy was assessed by comparing the EKF-based SOC trajectories with the experimentally derived reference SOC. The results are presented in terms of RMSE metrics and representative cycle comparisons.

4.3.1. EKF SOC Estimation Accuracy

The overall estimation accuracy of the EKF method is summarized using the RMSE values calculated over all evaluated cycles. The average errors obtained for the EKF estimator are:

- Charge RMSE: 0.0132 (1.32 %SOC)
- Discharge RMSE: 0.0149 (1.49 %SOC)
- Overall RMSE: 0.0143 (1.43 %SOC)

These values indicate a substantial improvement compared with the baseline Coulomb Counting method presented in Section 3.3. While the CC estimator exhibited an overall RMSE above 4% SOC, the EKF reduces the average estimation error to approximately 1.4% SOC, demonstrating the advantage of incorporating the battery voltage dynamics into the estimation process.

Figure 22 illustrates the evolution of the overall RMSE across the cycling experiment and compares the EKF performance with the Coulomb Counting baseline.

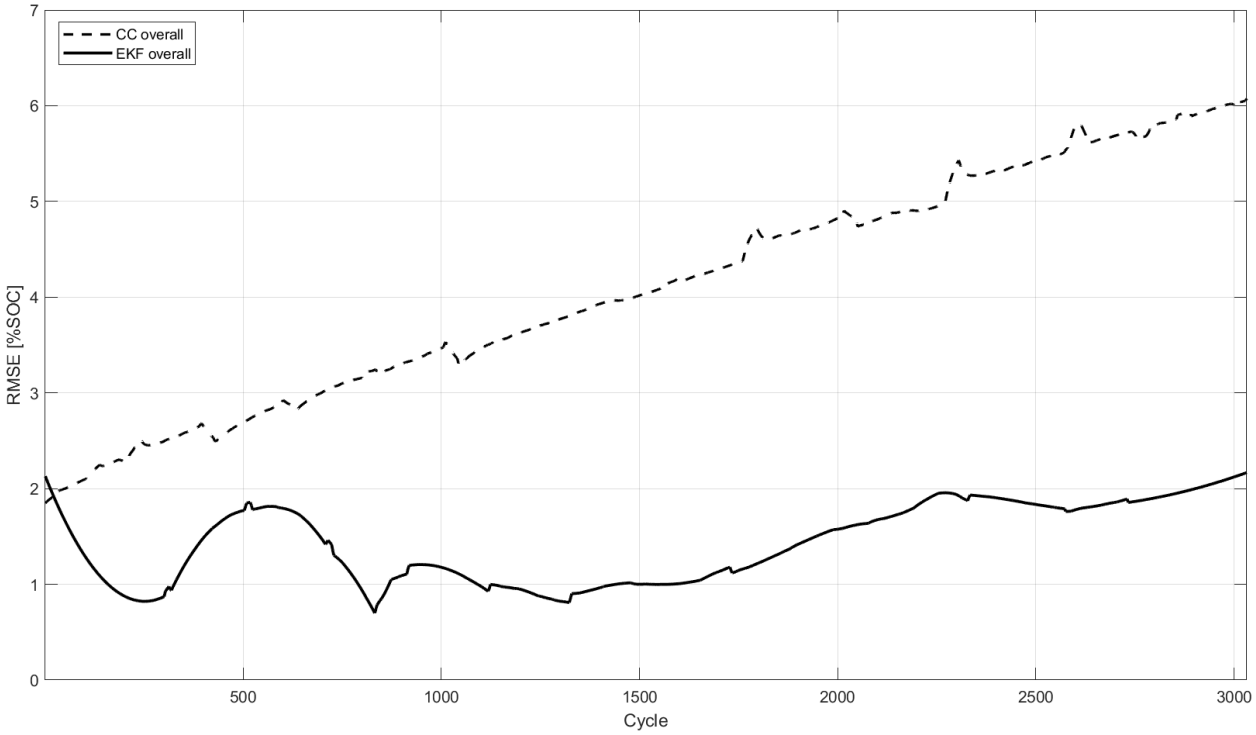

Figure 22: Comparison of RMSE evolution for the Coulomb Counting and EKF estimators across the dataset cycles.

As shown in the figure, the EKF estimator maintains a significantly lower error throughout the entire cycling experiment. While the Coulomb Counting error increases progressively with the cycle number due to the accumulation of integration errors, the EKF error remains relatively stable. This behavior confirms that the voltage-based correction mechanism effectively mitigates the drift that typically affects current-integration methods.

Although a slight increase in RMSE can still be observed toward the later stages of the dataset, the magnitude of this increase remains limited. Even at higher cycle numbers, the EKF error remains well below the corresponding Coulomb Counting error, highlighting the robustness of the model-based approach.

To further illustrate the estimation behavior, Figure 23 presents representative SOC trajectories for three cycles selected from the beginning, middle, and end of the dataset.

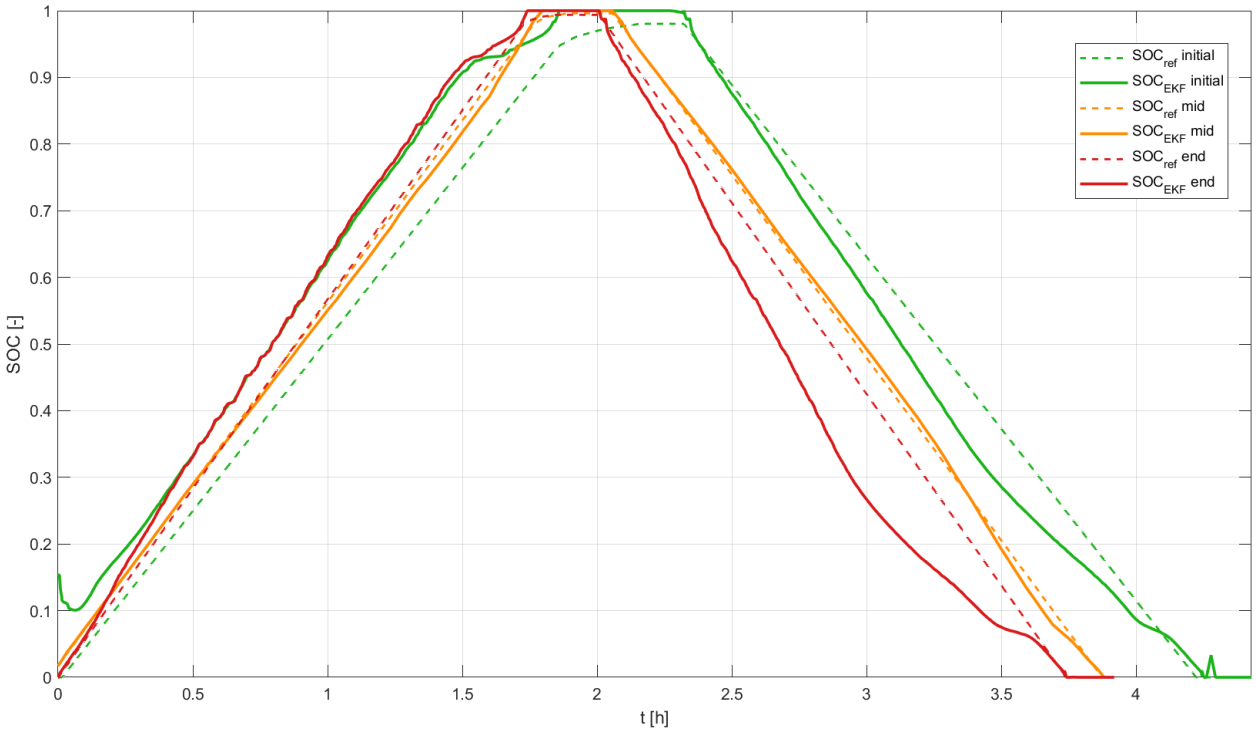

Figure 23: Comparison between reference SOC and EKF SOC estimates for representative cycles across the dataset.

The figure shows that the EKF estimator closely follows the reference SOC trajectory during both the charging and discharging phases. The agreement between the estimated and reference SOC curves remains good across the different stages of the battery lifecycle, indicating that the estimator is capable of maintaining stable performance over long-term cycling.

In the early cycle, the EKF estimate nearly overlaps with the reference SOC, demonstrating a highly accurate estimation when the battery parameters closely match the assumed model parameters. In the mid-life cycle, the EKF continues to track the SOC trajectory with only minor deviations. Even in the later cycle, where the reference SOC deviates more significantly from the baseline CC estimate, the EKF still maintains a relatively close correspondence with the reference trajectory.

4.3.2. EKF Error Analysis

A closer inspection of the EKF estimation error reveals several important characteristics of the estimator behavior.

First, the EKF significantly reduces the long-term drift that was observed in the Coulomb Counting method. Because the EKF periodically corrects the predicted SOC using the measured terminal voltage, the integration error does not accumulate indefinitely. Instead, the estimator continuously adjusts the SOC estimate to remain consistent with the observed battery voltage response.

Second, the estimation error remains relatively consistent between the charge and discharge phases. Unlike the Coulomb Counting method, which showed a pronounced asymmetry between charge and discharge errors, the EKF produces similar RMSE values for both phases. This indicates that the voltage-based correction mechanism is effective under both operating conditions.

Nevertheless, some estimation deviations can still be observed, particularly during the discharge phase of later cycles. These deviations may arise from several factors, including parameter mismatch in the equivalent circuit model, aging-related changes in the battery characteristics, and the reduced observability associated with the flat voltage plateau typical of LFP chemistry. In such regions, the derivative of the OCV–SOC curve becomes small, which reduces the sensitivity of the voltage measurement to SOC changes and therefore limits the effectiveness of the correction step in the Kalman filter.

Despite these limitations, the EKF estimator demonstrates a substantial improvement over the baseline method and provides a stable and accurate SOC estimation across the full dataset. The achieved accuracy of approximately 1.4% SOC RMSE confirms the effectiveness of the model-based estimation approach.

However, the remaining estimation error suggests that further improvements may still be possible. In particular, the residual estimation patterns observed in the EKF output motivate the introduction of a data-driven correction mechanism. The next section therefore investigates the proposed hybrid EKF–Neural Network framework, which aims to further reduce the SOC estimation error by learning the remaining structured residuals of the EKF estimator.

4.4. Hybrid EKF–Neural Network Estimation Results

The final stage of the experimental evaluation concerns the proposed hybrid SOC estimation framework that combines the Extended Kalman Filter with a neural-network-based residual correction. As described in Chapter 3, the neural network was trained to learn the residual error between the EKF SOC estimate and the reference SOC. The corrected hybrid estimate was then obtained by adding the predicted correction to the EKF output.

The performance of the hybrid estimator was evaluated using the test cycles defined in the validation protocol described in Section 4.1. In order to ensure the integrity of the evaluation and to avoid data leakage, only the cycles belonging to the test subset were used for the final performance assessment. Cycles that were used for neural network training or validation were excluded from the evaluation.

Because the RMSE curves shown in this section are computed strictly over the test subset, the trend of the lines may differ slightly from the earlier EKF-only evaluation presented in Section 4.3, which considered the entire dataset. However, the overall trend and the relative performance improvements remain consistent.

The following sections analyze the hybrid estimator performance and quantify the error reduction achieved with respect to the standalone EKF method.

4.4.1. Hybrid SOC Estimation Performance

The accuracy of the hybrid SOC estimator was evaluated using the same RMSE metrics defined in Section 4.1. The average RMSE values computed over the test cycles are summarized below:

- Charge RMSE (Hybrid): 0.0107 (1.07 %SOC)
- Discharge RMSE (Hybrid): 0.0084 (0.84 %SOC)
- Overall RMSE (Hybrid): 0.0097 (0.97 %SOC)

These results indicate that the hybrid framework consistently improves the SOC estimation accuracy across all operating phases. In particular, the hybrid estimator reduces the overall RMSE to below 1% SOC, demonstrating the effectiveness of combining model-based estimation with a data-driven correction mechanism.

Figure 24 shows the evolution of the overall RMSE across the cycling experiment for the three considered estimators: Coulomb Counting, EKF, and the proposed hybrid method.

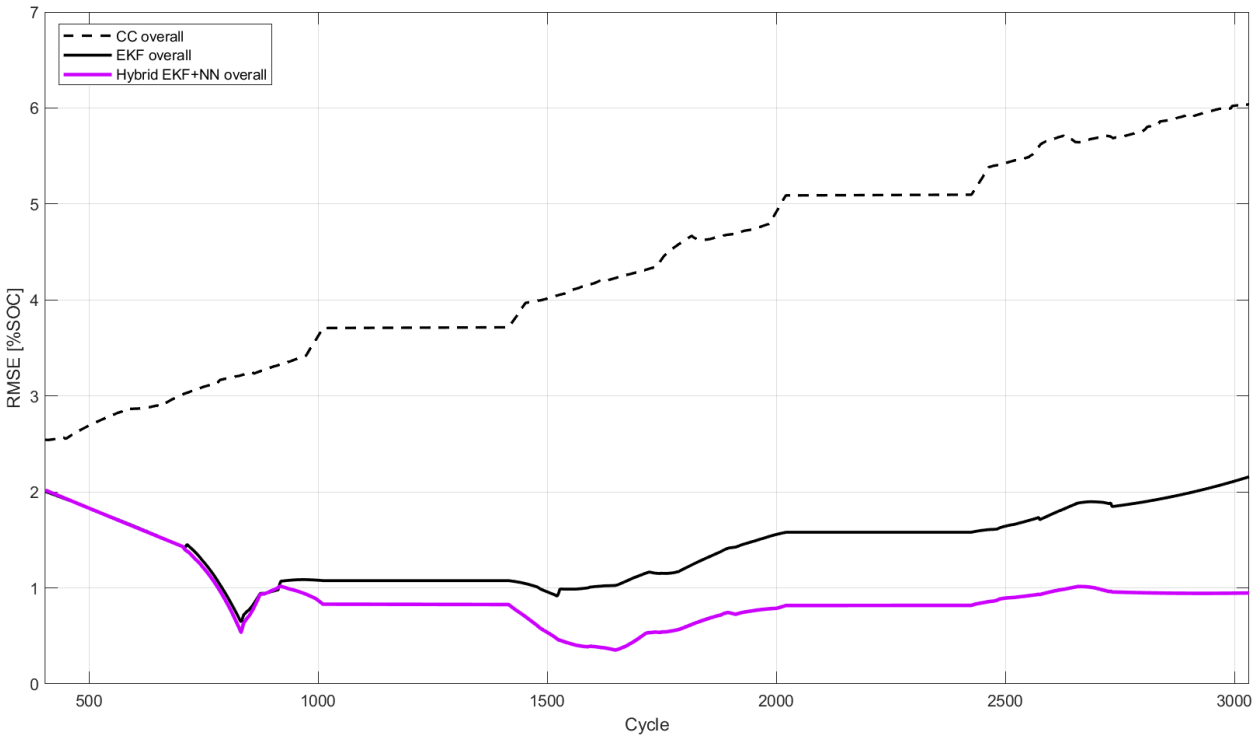

Figure 24: Comparison of RMSE evolution for Coulomb Counting, EKF, and the hybrid EKF–Neural Network estimator across test cycles.

The figure clearly illustrates the performance hierarchy of the three approaches. The Coulomb Counting estimator exhibits the largest error and a clear upward trend across the cycles due to cumulative integration errors. The EKF significantly reduces the estimation error by incorporating voltage measurements and battery model dynamics. The hybrid estimator further improves the performance by compensating for the residual errors of the EKF.

The RMSE curve of the hybrid method remains consistently below that of the standalone EKF throughout the dataset. Furthermore, the hybrid estimator shows a more stable error profile over the entire lifecycle of the battery, indicating that the learned correction mechanism remains effective even as the battery characteristics evolve with cycling.

To further illustrate the estimation behavior, several representative test cycles are shown in Figures 25–27.

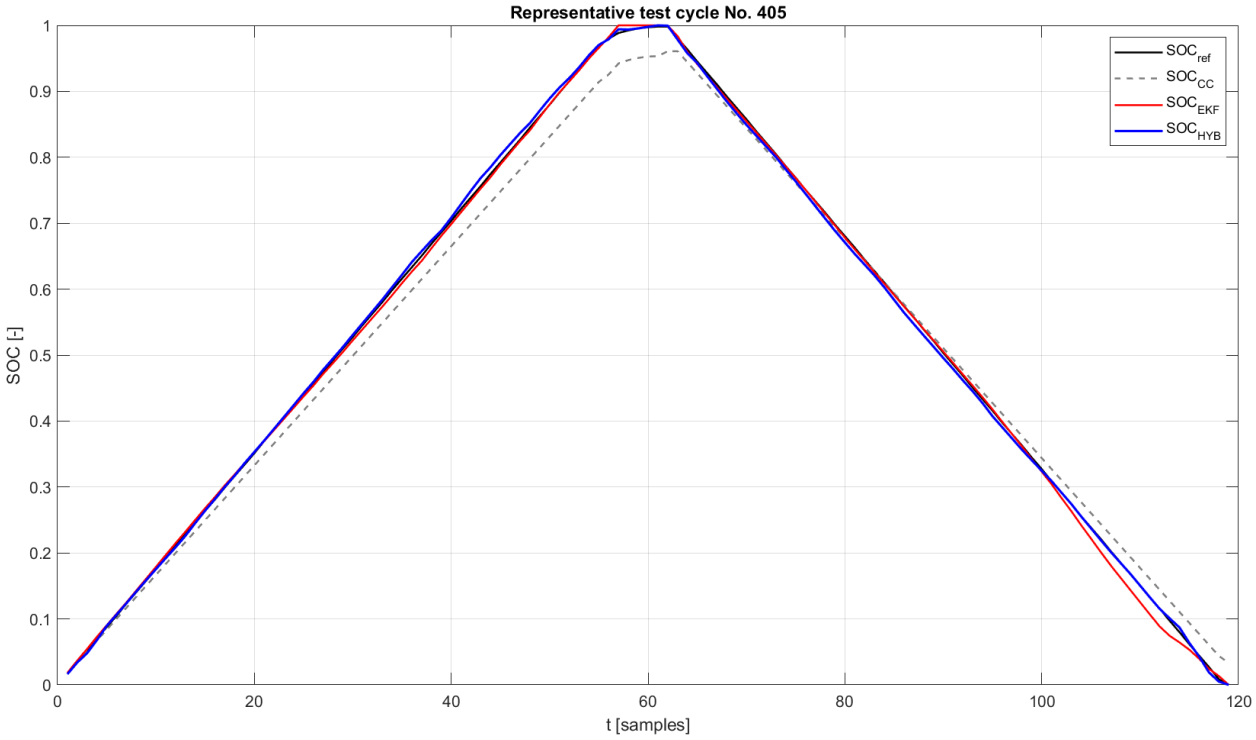

Figure 25: SOC trajectories for representative test cycle 405.

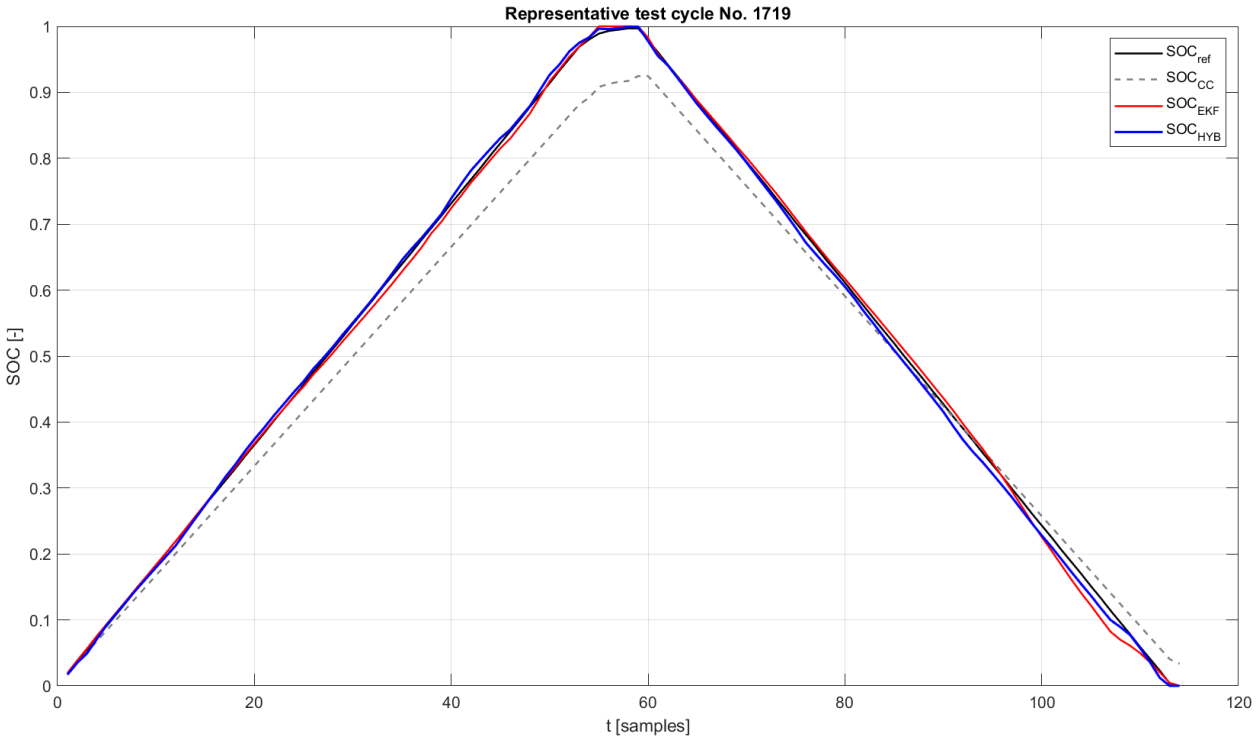

Figure 26: SOC trajectories for representative test cycle 1719.

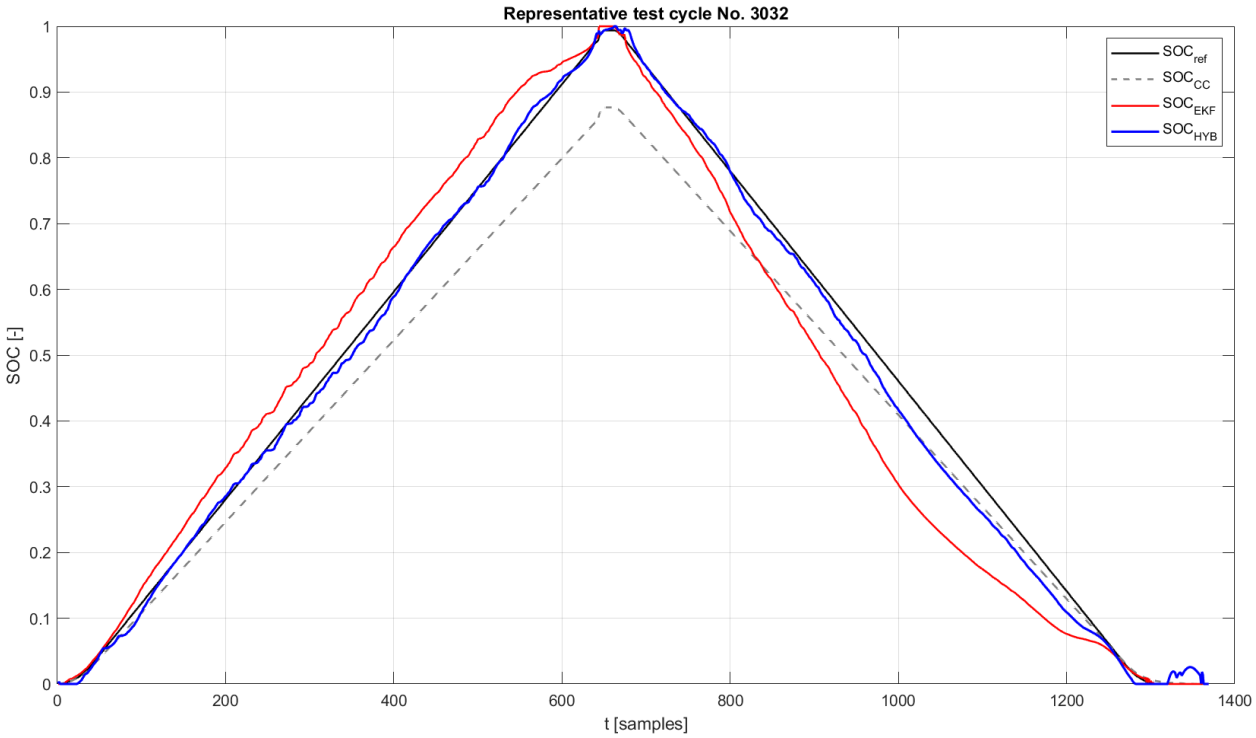

Figure 27: SOC trajectories for representative test cycle 3032.

Each figure compares the reference SOC with the estimates produced by Coulomb Counting, the EKF, and the hybrid estimator.

For the early test cycle (cycle 405), all estimation methods follow the general SOC trajectory, but the Coulomb Counting method shows a visible deviation due to integration drift. The EKF estimate closely tracks the reference SOC, while the hybrid estimator further improves the alignment, particularly during the discharge phase.

In the mid-life cycle (cycle 1719), the limitations of the Coulomb Counting method become more pronounced. The EKF continues to provide a significantly better estimate, while the hybrid approach further refines the trajectory by correcting the remaining EKF deviations.

The differences become even more evident in the late-life cycle (cycle 3032). In this case, the EKF begins to exhibit larger deviations from the reference SOC during the discharge phase, which can be attributed to model mismatch and changes in the battery characteristics over time. The hybrid estimator partially compensates for this effect by adjusting the EKF prediction, resulting in a closer match with the reference trajectory.

These representative examples confirm that the hybrid framework successfully captures structured residual errors of the EKF and improves the SOC estimation accuracy across different stages of the battery lifecycle.

4.4.2. Error Reduction Compared to EKF

The improvement achieved by the hybrid estimator can be quantified by comparing the RMSE values obtained with the EKF and the hybrid method.

For the charge phase, the RMSE decreases from 1.38% SOC to 1.07% SOC, corresponding to an improvement of approximately 22%.

For the discharge phase, the improvement is even more pronounced, with the RMSE decreasing from 1.56% SOC to 0.84% SOC, which corresponds to an error reduction of approximately 46%.

Considering the full cycle evaluation, the overall RMSE decreases from 1.49% SOC for the EKF to 0.97% SOC for the hybrid estimator, corresponding to an improvement of approximately 35%.

These results demonstrate that the neural-network-based correction is particularly effective in compensating for residual EKF errors that arise from modeling limitations and battery nonlinearities. In particular, the largest improvements are observed during the discharge phase, where the voltage response of LFP batteries may reduce the observability of SOC for model-based estimators.

Overall, the results confirm that the proposed hybrid EKF–Neural Network framework successfully combines the strengths of model-based estimation and data-driven learning. The EKF provides a physically consistent baseline estimate, while the neural network learns to correct the remaining estimation error, resulting in a more accurate and robust SOC estimation across the entire dataset.

4.5. Comparative Performance Analysis

After evaluating the individual estimation approaches separately, a comparative analysis was performed in order to quantify the relative performance of the three considered SOC estimation methods: the Coulomb Counting baseline, the model-based EKF estimator, and the proposed hybrid EKF–Neural Network framework.

The comparison focuses on the RMSE values obtained for the charge phase, the discharge phase, and the overall cycle evaluation. By analyzing the estimation accuracy across these operating conditions, it becomes possible to assess the benefits introduced by each methodological improvement.

The results summarized in this section provide a consolidated view of the estimation performance and highlight the progressive improvements achieved when moving from a purely integration-based method to a model-based estimator and finally to a hybrid physics–data-driven framework.

4.5.1. RMSE Comparison Across Methods

Table 3 summarizes the RMSE values obtained for the three estimation approaches. The results clearly illustrate the progressive improvement in SOC estimation accuracy achieved by incorporating additional modeling and learning capabilities.

Method	Charge RMSE (%SOC)	Discharge RMSE (%SOC)	Overall RMSE (%SOC)
Coulomb Counting (CC)	**5.01**	**2.77**	**4.09**
Extended Kalman Filter (EKF)	**1.32**	**1.49**	**1.43**
Hybrid EKF–NN	**1.07**	**0.84**	**0.97**

Table 3: RMSE comparison of SOC estimation methods for charge, discharge, and overall operation.

The baseline Coulomb Counting method exhibits the largest estimation error across all operating conditions. In particular, the charge RMSE exceeds 5% SOC, reflecting the accumulation of integration errors and the sensitivity of the method to capacity mismatch over long-term cycling.

The EKF estimator significantly improves the estimation accuracy by incorporating voltage measurements through the equivalent circuit model. As shown in Table 3, the overall RMSE decreases to approximately 1.43% SOC, representing a substantial improvement over the baseline method.

The hybrid EKF–Neural Network framework further enhances the estimation accuracy. By learning the residual error patterns of the EKF estimator, the hybrid model reduces the overall RMSE to 0.97% SOC, achieving sub-1% SOC accuracy under the considered experimental conditions.

Figure 28 provides a visual comparison of the RMSE values for the different estimation approaches.

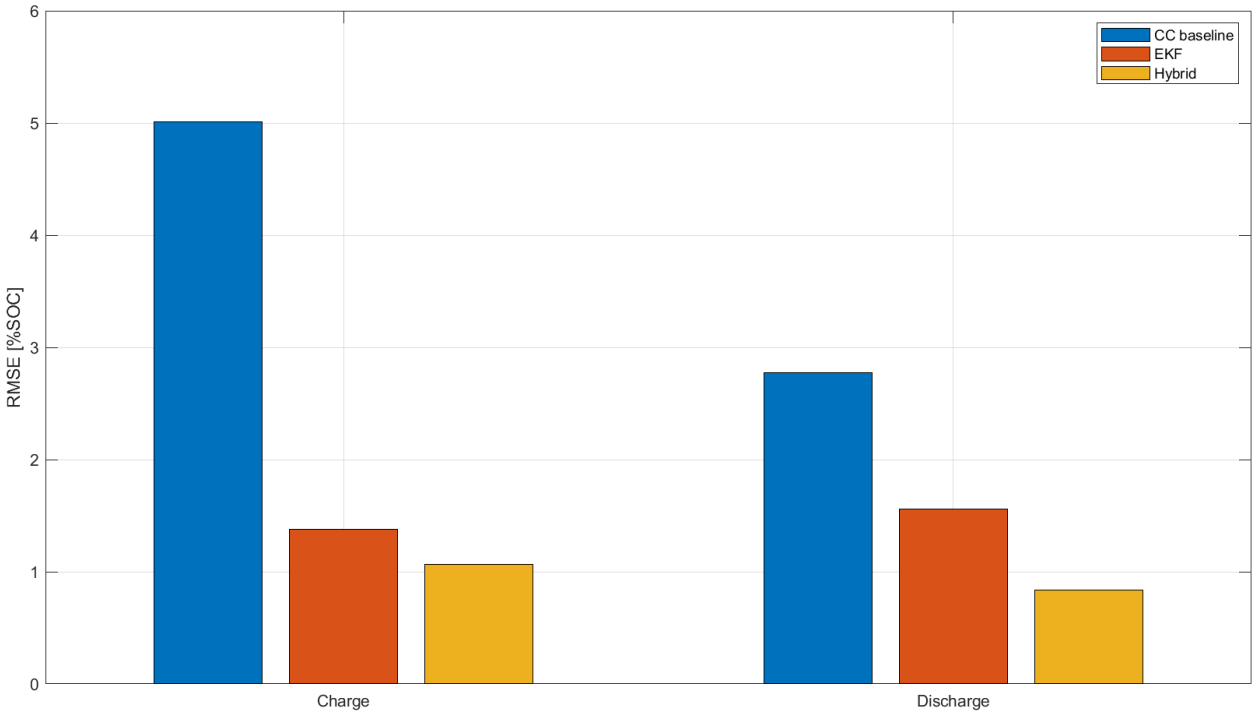

Figure 28: RMSE comparison between Coulomb Counting, EKF, and Hybrid SOC estimators.

The figure highlights the progressive reduction in estimation error when moving from the CC baseline to the EKF estimator and finally to the hybrid framework. The improvement is particularly noticeable in the charging phase, where the Coulomb Counting method exhibits the largest error.

4.5.2. Performance Gain of the Hybrid Framework

In order to quantify the performance improvement provided by each method, the gain between different estimators was evaluated using the following metric:

$$Gain = \frac{RMSE_{reference}}{RMSE_{improved}}$$

This metric indicates how many times the estimation error is reduced when moving from one estimation method to another.

The comparison between the Coulomb Counting and EKF estimators shows a substantial improvement obtained through the introduction of the model-based observer. The EKF reduces the estimation error by:

- 3.80× during the charge phase
- 1.85× during the discharge phase
- 2.85× in the overall evaluation

These results demonstrate that incorporating the battery voltage dynamics through the equivalent circuit model significantly improves SOC estimation accuracy compared with current integration alone.

The proposed hybrid EKF–Neural Network framework provides an additional performance improvement by correcting the residual EKF estimation error. The hybrid estimator achieves the following gains relative to the EKF:

- 1.29× improvement during charge
- 1.86× improvement during discharge
- 1.53× improvement in overall RMSE

The improvement is particularly pronounced during the discharge phase, where the neural-network correction significantly reduces the remaining estimation error of the EKF estimator.

5. Discussion

This chapter provides an interpretation of the results presented in Chapter 4 and discusses the implications of the obtained performance for SOC estimation in lithium iron phosphate batteries. The discussion focuses on the behavior of the hybrid estimation framework, the limitations related to the electrochemical characteristics of LFP cells, and the practical considerations of the proposed method.

5.1. Interpretation of Hybrid Estimator Performance

The results obtained in this study demonstrate a clear progression in SOC estimation accuracy when moving from a purely integration-based method to a model-based estimator and finally to a hybrid framework that combines physical modeling with data-driven learning.

The Coulomb Counting approach shows the largest estimation error among the evaluated methods. Although this method is widely used due to its simplicity and low computational cost, it suffers from inherent limitations related to error accumulation. Any bias in the current measurement or uncertainty in the battery capacity leads to a cumulative integration error that gradually increases over time. This behavior was clearly observed in the experimental results, where the estimation error increased progressively across the dataset as the number of cycles increased.

The Extended Kalman Filter significantly improves the estimation accuracy by incorporating voltage measurements and battery dynamics through the equivalent circuit model. The EKF combines the prediction of SOC through current integration with a correction step based on voltage feedback. This feedback mechanism allows the filter to compensate for the long-term drift observed in the Coulomb Counting method. As a result, the EKF maintains a relatively stable estimation error across the entire battery lifecycle and achieves a substantial reduction in RMSE compared with the baseline method.

Despite this improvement, residual errors remain in the EKF estimates. These residual errors arise from model simplifications, parameter uncertainties, and the nonlinear behavior of the battery that cannot be fully captured by a simplified equivalent circuit model. The hybrid EKF–Neural Network framework addresses these residual errors by introducing a data-driven correction stage.

In the proposed architecture, the EKF provides a physically consistent baseline estimate of the SOC, while the neural network learns the residual error between the EKF estimate and the reference SOC. By modeling this residual error directly from experimental data, the neural network is able to capture systematic estimation biases that are difficult to represent using analytical models alone.

The results demonstrate that this residual learning strategy effectively improves the estimation accuracy. The hybrid estimator achieves the lowest RMSE among the evaluated methods and consistently reduces the estimation error across the entire range of battery cycles. Importantly, the hybrid framework does not replace the physical model but rather complements it, preserving the interpretability and robustness of the EKF while enhancing its accuracy through data-driven correction.

5.2. Observability Limitations in LFP Batteries

An important factor influencing the performance of SOC estimation algorithms is the observability of the battery state from the measured electrical signals. In lithium iron phosphate batteries, the voltage profile exhibits a characteristic flat plateau over a large portion of the SOC range. In this region, the derivative of the open-circuit voltage with respect to SOC is very small.

This property significantly limits the amount of information about SOC that can be extracted from the voltage measurement. When the OCV–SOC slope is small, even relatively large variations in SOC result in only minor changes in terminal voltage. As a consequence, the voltage-based correction step in model-based observers such as the EKF becomes less effective.

This limited observability is one of the main reasons why residual estimation errors remain even after applying a model-based filtering approach. Small modeling inaccuracies, parameter deviations, or measurement noise may lead to persistent SOC estimation errors when the voltage signal does not provide sufficient information to correct them.

The hybrid estimation framework partially mitigates this limitation by learning residual patterns directly from the data. While the neural network does not change the physical observability of the system, it is able to exploit statistical correlations between the measured signals and the residual estimation error. In this way, the hybrid approach improves the effective estimation accuracy even in regions where the physical model alone provides limited correction capability.

5.3. Limitations of the Proposed Method

Although the proposed hybrid estimation framework demonstrates promising performance, several limitations of the present study should be acknowledged.

First, the experimental validation was performed using a dataset obtained under controlled laboratory conditions. The cycling experiments were conducted using relatively structured current profiles based on constant-current charge and discharge phases. While this type of testing is suitable for methodological evaluation, real-world battery operation often involves highly dynamic load profiles, such as those encountered in electric vehicles or grid applications. Additional

validation under dynamic current profiles would therefore be necessary to assess the robustness of the proposed framework under realistic operating conditions.

Second, the equivalent circuit model used in the EKF implementation relies on fixed parameters. In practical battery systems, these parameters may vary with temperature, state of health, and operating conditions. Changes in internal resistance or polarization dynamics may influence the accuracy of the model-based estimation. Incorporating adaptive parameter identification or joint state–parameter estimation techniques could further improve the robustness of the proposed framework.

Finally, the neural network was trained using data from the same experimental dataset used for evaluation, although strict separation between training, validation, and testing cycles was enforced to avoid data leakage. Nevertheless, further evaluation on independent datasets would provide a more comprehensive assessment of the generalization capability of the hybrid estimator.

5.4. Computational Considerations

From a practical perspective, the computational complexity of SOC estimation algorithms is an important factor for their implementation in battery management systems.

The Coulomb Counting method has the lowest computational cost, as it only requires simple numerical integration of the current signal. However, this simplicity comes at the cost of limited accuracy and poor robustness over long operating periods.

The EKF estimator introduces additional computational requirements due to the matrix operations involved in the prediction and update steps. Nevertheless, the state dimension of the implemented equivalent circuit model is relatively small, consisting of the SOC state and the polarization voltage state. As a result, the computational burden of the EKF remains moderate and is well within the capabilities of typical microcontrollers used in modern battery management systems.

The hybrid EKF–Neural Network framework adds an additional inference step corresponding to the neural network correction. However, the neural network used in this work has a relatively compact architecture, which limits the additional computational overhead. During operation, the neural network performs only forward inference, which is computationally inexpensive compared with the training process.

Therefore, despite the additional complexity introduced by the hybrid framework, the proposed approach remains suitable for practical implementation in real-time battery management systems. The combination of moderate computational cost and improved estimation accuracy makes the hybrid EKF–Neural Network framework a promising candidate for advanced SOC estimation applications.

6. Conclusion

This thesis addressed the problem of accurate state-of-charge (SOC) estimation for lithium iron phosphate (LFP) batteries by combining model-based estimation with data-driven learning. Reliable SOC estimation is essential for battery management systems, yet the flat voltage plateau characteristic of LFP chemistry significantly limits the observability of SOC using voltage measurements alone.

An SOC estimation framework was developed and evaluated through three progressively advanced approaches: Coulomb Counting, model-based estimation using an Extended Kalman Filter (EKF), and a hybrid EKF–Neural Network estimator.

The experimental dataset obtained from a cylindrical 18650 LFP cell was first preprocessed and segmented into individual charge–discharge cycles. A reference SOC trajectory was constructed and used as ground truth for performance evaluation.

Coulomb Counting was implemented as a baseline estimator. Although computationally simple, the method exhibited the expected integration drift, leading to cumulative estimation errors across the dataset. The resulting overall estimation error reached 4.09% SOC RMSE, confirming the limitations of current-integration methods for long-term SOC tracking.

A model-based estimator based on the Extended Kalman Filter was then developed using a Thevenin equivalent circuit model and an experimentally derived OCV–SOC relationship. By incorporating voltage measurements into the correction step, the EKF significantly reduced the estimation error, achieving an overall accuracy of 1.43% SOC RMSE.

To further improve the estimation accuracy, a hybrid EKF–Neural Network framework was proposed. In this architecture, a recurrent neural network learns the residual error between the EKF estimate and the reference SOC, and the predicted correction is applied to the EKF output. The experimental results show that this hybrid approach reduces the overall estimation error to 0.97% SOC RMSE, achieving sub-1% SOC accuracy.

The results demonstrate that combining physics-based observers with data-driven residual learning provides an effective strategy for improving SOC estimation. The EKF ensures physical consistency and robustness, while the neural network compensates for structured residual errors that arise from model simplifications and limited observability.

Overall, the proposed hybrid estimation framework demonstrates that integrating model-based observers with machine learning techniques can significantly enhance SOC estimation accuracy for lithium iron phosphate batteries. This approach provides a promising direction for the development of more reliable and intelligent battery management systems in future energy storage applications.

7. Future Work

Several directions can be identified to extend the work presented in this thesis.

First, further validation of the proposed framework under dynamic current profiles would provide a more realistic assessment of the estimator performance. Real battery applications often involve highly dynamic load conditions, such as electric vehicle driving cycles, which differ from the structured cycling profiles used in this study.

Second, the equivalent circuit model parameters were assumed constant in the present implementation. In practical battery systems, these parameters may vary with temperature, aging, and operating conditions. Incorporating adaptive parameter identification or joint state–parameter estimation techniques could improve the robustness of the model-based estimation stage.

Another potential extension involves incorporating additional input features into the neural network model, such as temperature measurements or state-of-health indicators. These variables may allow the neural network to capture more complex residual dynamics and further improve the accuracy of the hybrid estimator.

Finally, the implementation of the proposed hybrid framework in an embedded battery management system represents an important step toward practical deployment. Given the relatively moderate computational requirements of the EKF and the compact neural network architecture used in this work, real-time implementation on typical BMS hardware appears feasible.

Further research along these directions could contribute to the development of more adaptive, robust, and accurate battery state estimation methods for next-generation energy storage systems.

Bibliography

[1] M. Armand and J.-M. Tarascon, “Building better batteries,” *Nature*, vol. 451, pp. 652–657, 2008.

[2] International Energy Agency (IEA), *Global EV Outlook 2023*, Paris: IEA, 2023.

[3] G. L. Plett, “Extended Kalman filtering for battery management systems of LiPB-based HEV battery packs: Part 1–3,” *Journal of Power Sources*, vol. 134–136, 2004.

[4] X. Hu, S. Li, and H. Peng, “A comparative study of equivalent circuit models for Li-ion batteries,” *Journal of Power Sources*, vol. 198, pp. 359–367, 2012.

[5] M. Wei et al., “Robust state of charge estimation of LiFePO4 batteries based on Sage–Husa adaptive Kalman filter and dynamic neural network,” *Electrochimica Acta*, vol. 477, p. 143778, 2024.

[6] Y. Che et al., “Enhanced SOC Estimation for LFP Batteries: A Synergistic Approach Using Coulomb Counting Reset, Machine Learning, and Relaxation,” *ACS Energy Letters*, vol. 10, pp. 741–749, 2025.

[7] X. Yun et al., “A review on state of charge estimation methods for lithium-ion batteries based on data-driven and model fusion,” *Journal of Energy Storage*, vol. 129, 117389, 2025.

[8] H. He, R. Xiong, and J. Fan, “Evaluation of lithium-ion battery equivalent circuit models for state of charge estimation,” *Applied Energy*, vol. 88, no. 11, pp. 4134–4141, 2011.

[9] G. L. Plett, “Sigma-point Kalman filtering for battery management systems of LiPB-based HEV battery packs,” *Journal of Power Sources*, vol. 161, pp. 1356–1368, 2006.

[10] H. He, R. Xiong, X. Zhang, F. Sun, and J. Fan, “State-of-charge estimation of the lithium-ion battery using an adaptive extended Kalman filter based on an improved Thevenin model,” *IEEE Transactions on Vehicular Technology*, vol. 60, no. 4, pp. 1461–1469, 2011.

[11] X. Hu, S. Li, and H. Peng, “A comparative study of equivalent circuit models for Li-ion batteries,” *Journal of Power Sources*, vol. 198, pp. 359–367, 2012.

[12] M. Dubarry, C. Truchot, and B. Y. Liaw, “Synthesize battery degradation modes via a diagnostic and prognostic model,” *Journal of Power Sources*, vol. 219, pp. 204–216, 2012.

[13] R. Xiong, H. He, F. Sun, and K. Zhao, “Evaluation on state of charge estimation of batteries with adaptive extended Kalman filter,” *Energy*, vol. 39, pp. 310–318, 2012.

[14] G. L. Plett, “Extended Kalman filtering for battery management systems of LiPB-based HEV battery packs: Part 2,” *Journal of Power Sources*, vol. 134, pp. 262–276, 2004.

[15] S. Julier and J. Uhlmann, “Unscented filtering and nonlinear estimation,” *Proceedings of the IEEE*, vol. 92, no. 3, pp. 401–422, 2004.

[16] H. E. Perez, X. Hu, S. Dey, and S. Moura, “Optimal sensor placement for fault detection in lithium-ion batteries,” *IEEE Transactions on Control Systems Technology*, vol. 23, no. 2, pp. 734–743, 2015.

[17] M. Wei et al., “Robust state of charge estimation of LiFePO4 batteries based on Sage–Husa adaptive Kalman filter and dynamic neural network,” *Electrochimica Acta*, vol. 477, 143778, 2024.

[18] Y. Tian, D. Li, and J. Yang, “State-of-charge estimation of lithium-ion batteries using LSTM networks,” *Energy*, vol. 172, pp. 1–11, 2019.

[19] X. Zhang, Y. Wang, and C. Zhang, “Lithium-ion battery SOC estimation using a deep neural network,” *Applied Energy*, vol. 250, pp. 547–558, 2019.

[20] M. A. Hannan et al., “State-of-charge estimation of lithium-ion battery using recurrent neural network,” *Energies*, vol. 11, no. 6, 2018.
[21] X. Li, L. Zhang, and J. Wang, “Hybrid LSTM–Kalman filtering method for SOC estimation of lithium-ion batteries,” *Journal of Energy Storage*, vol. 40, 102699, 2021.
[22] X. Yun et al., “A review on state of charge estimation methods for lithium-ion batteries based on data-driven and model fusion,” *Journal of Energy Storage*, vol. 129, 117389, 2025.
[23] Y. Che et al., “Enhanced SOC Estimation for LFP Batteries: A Synergistic Approach Using Coulomb Counting Reset, Machine Learning, and Relaxation,” *ACS Energy Letters*, vol. 10, pp. 741–749, 2025.
[24] M. Safari and C. Delacourt, “Modeling of a commercial graphite/LiFePO4 cell,” *Journal of the Electrochemical Society*, vol. 158, no. 5, 2011.
[25] P. Ramadass, B. Haran, P. M. Gomadam, R. White, and B. N. Popov, “Development of first principles capacity fade model for Li-ion cells,” *Journal of the Electrochemical Society*, 2004.
[26] S. Santhanagopalan and R. E. White, “Online estimation of the state of charge of a lithium ion cell,” *Journal of Power Sources*, vol. 161, 2006.
[27] Y. Zeng, J. Li, and C. Wang, “SOC estimation of lithium-ion batteries based on UKF and LSTM,” *Energy*, vol. 189, 2019.
[28] H. Hou, Y. Zou, and X. Wang, “State-of-charge estimation of lithium-ion batteries based on EKF and XGBoost,” *Applied Energy*, vol. 253, 2019.
[29] J. Liu et al., “Closed-loop SOC estimation combining Kalman filtering and neural networks,” *Energy Storage Materials*, vol. 22, 2019.
[30] X. Cui, Y. Zhang, and H. Chen, “Improved GRU–UKF hybrid method for lithium-ion battery state estimation,” *Journal of Energy Storage*, vol. 48, 103920, 2022.